

2005

Open microstrip line leaky-wave antenna

Hai Jiang
University of Dayton

Follow this and additional works at: https://ecommons.udayton.edu/graduate_theses

Recommended Citation

Jiang, Hai, "Open microstrip line leaky-wave antenna" (2005). *Graduate Theses and Dissertations*. 3548.
https://ecommons.udayton.edu/graduate_theses/3548

This Thesis is brought to you for free and open access by the Theses and Dissertations at eCommons. It has been accepted for inclusion in Graduate Theses and Dissertations by an authorized administrator of eCommons. For more information, please contact mschlange1@udayton.edu, ecommons@udayton.edu.

Open Microstrip Line Leaky-wave Antenna

A Thesis

Submitted to

The School of Engineering of the

UNIVERSITY OF DAYTON

In Partial Fulfillment of the Requirements for

The Degree

Master of Science in Electrical Engineering

by

Hai Jiang

UNIVERSITY OF DAYTON

Dayton, Ohio

December, 2005

Open Microstrip Line Leaky-wave Antenna

*Hickman -
Please do not
remove this note!
Original*

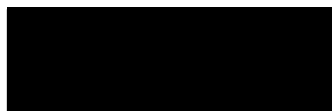
APPROVED BY:



Krishna M. Pasala, Ph.D.
Advisory Committee Chairman
Professor
Department of Electrical and
Computer Engineering



Robert Penno, Ph.D.
Committee Member
Associate Professor
Department of Electrical and
Computer Engineering



Guru Subramanyam, Ph.D
Committee Member
Associate Professor
Department of Electrical and Computer Engineering



Donald L. Moon, Ph.D.
Associate Dean
Graduate Engineering Program &
Research, School of Engineering



Joseph E. Saliba, Ph.D., P.E.
Dean, School of Engineering

To my parents, grandmother and my wife Xiaoyan.

ACKNOWLEDGMENTS

I would like to express my gratitude to all those who made it possible for me to complete this thesis. My foremost thanks goes to my adviser Dr. Krishna M. Pasala of University of Dayton, who introduced and helped me to start my research life in the fields of Antenna Design. Without him, this dissertation would not have been possible. His serious academic attitude and integral view on research made a deep impression on me and also influenced me significantly. I owe him a debt of gratitude for showing me how to conduct research. Besides being an excellent supervisor, professor Pasala is as close as a relative and also a good friend to me. I am really glad that I got to know professor Pasala in my life.

I am deeply indebted to Dr. Leo Kempel of Michigan State University without whose help the FEM analysis of LW antenna would not have been possible. I wish to thank Dr. Stephen Schneider whose support and technical discussions have been invaluable. I would also like to thank the rest of my thesis committee members: Dr. Robert Penno, Dr. Guru Subramanyam. Their valuable feedback helped me to improve the thesis in many ways.

A special thanks to Chunlei and his wife Ran for their generous help. I am grateful to Chunlei for his help and important advice in writing this thesis. I also want to thank all the friends I met in Dayton, Gary Miao, Water, Hao, Zhitong and Yufen, Zhanxiong, Hua Jiang, Xiaolu and Yiyang who gave me a lot of help.

Especially, I would like to give my thanks to my wife Xiaoyan whose patient love and encouragement enabled me to complete this work.

Finally, I wish to thank my parents and my grandmother. All the work I did in the past would not be possible without them and also in the future.

ABSTRACT

For many air-borne applications, such as in Avionics, it is advantageous to have antennas which are light-weight, have a low profile and high bandwidth. It is also desirable for these antennas to be capable of low-angle radiation, towards horizon. Printed leaky wave antennas meet these requirements and are considered here. The specific configuration considered here consists of an open microstrip excited asymmetrically to realize the first higher mode and was discussed first by Menzel[1]. This can also be realized in "half-width" configuration and was considered by Zelinsky[2], who used the FDTD approach to analyze this antenna. In the present work, we developed analytical expressions for the propagation constant and the fields in microstrip and use the Finite Elements (FE) method as a tool to validate the theory. Excellent agreement between theoretical and simulated results is obtained and the theory is used to determine the wave and driving point impedances. The calculated driving point impedance may be used to terminate the antenna to absorb the residual power and minimize the reflections. The FE approach is especially suitable to simulate and analyze inhomogeneous dielectric structures. It is demonstrated that by periodically loading the microstrip line with air gaps and keeping the period much less than a wavelength, it is possible to control the characteristics of the leaky wave mode and realize a leaky wave antenna whose band-width is increased by a factor of 50% or more compared to the homogeneous substrate antenna while leaving the pattern characteristics essentially unchanged.

TABLE OF CONTENTS

	Page
Abstract	vi
List of Figures	ix
Chapters:	
1. Introduction	1
2. Leaky Wave Phenomenon	5
2.1 Basic Definition	5
2.2 Introductory Principles of Leaky Wave	6
3. Theoretical Analysis of Leaky Waves in Microstrip	10
3.1 An Oblique Incident TEM Wave in a Parallel-plate Waveguide . . .	10
3.2 Transverse Resonance Method	12
3.3 An Explicit Expression for the Propagation Constant of An Open Microstrip	14
3.4 Leaky Modes on Microstrip Line Antenna	17
3.5 Driving Point Impedance of the First Higher Mode in the Open Microstrip Line	19
3.5.1 Fields and Modes in the Open Microstrip Line	19
3.5.2 Driving Point Impedance of the First Higher Mode	22
4. Results: Simulation	26
4.1 Menzel's Antenna	26
4.1.1 Full-width Microstrip Line Leaky Wave Antenna with Two Symmetrical Feeds	29
4.1.2 Half Width Microstrip Line Leaky Wave Antenna with Single Feed	31
4.1.3 Bandwidth	33

4.2	Computed Propagation Constant Compared with the Theoretical Analysis	34
4.3	Field Distribution Obtained by Simulation Compared with Theoretical Analysis	36
4.4	Full-Width Microstrip Line Leaky Wave Antenna with Inhomogeneous Dielectric Materials	38
4.4.1	Bandwidth Enhancement	38
4.4.2	Inhomogeneous Substrate Leaky Wave Antenna	40
5.	Summary and Conclusions	47
	Bibliography	49

LIST OF FIGURES

Figure	Page
1.1 Normalized phase constant β/k_0 versus frequency f for the lowest mode and the first two higher modes in microstrip line with a top cover. The solid lines given by Ermert represent real wave numbers, whereas the dashed lines are corresponding to the real parts of the phase constant of the leaky mode solution in the radiation region. The dimensions of this microstrip line are width 3.00mm, dielectric layer thickness 0.635mm, $\epsilon_r = 9.80$, and the height of the top cover is 5 times the dielectric layer thickness.	2
1.2 Normalized Phase constant β/k_0 versus frequency for the first three higher modes of open microstrip line.	3
1.3 Normalized attenuation constant α/k_0 versus frequency for the first three higher modes of open microstrip line.	4
2.1 Two dimension figure for forward leaky wave	6
3.1 TEM wave incident onto the left boundary of a microstrip line or a dielectric filled parallel-plate waveguide.	11
3.2 Transverse Section of waveguide or microstrip (Z_{01} and Z_{02} are the characteristic impedances).	12
3.3 Normalized phase constant β/k_0 versus frequency for the first three higher modes of an open microstrip line. The dimensions of our microstrip line are thickness of the substrate 0.787mm, the patch width 15mm, dielectric constant $\epsilon_r = 2.33$	17
3.4 Normalized phase constant α/k_0 versus frequency for the first three higher modes of an open microstrip line. The dimensions of our microstrip line are thickness of the substrate 0.787mm, the patch width 15mm, dielectric constant $\epsilon_r = 2.33$	18

3.5	Bandwidth of microstrip line leaky-wave antenna by the Transverse Resonance Method.	19
3.6	Transverse section of an open microstrip line	19
3.7	Analytical Results for the Driving Point Impedance for the first higher mode in z direction. The blue line represents the real part of Z_z . The dashed red line represents the imaginary part of Z_z	23
3.8	Analytical Results for the driving point Impedance for the first higher mode in z direction. The blue line represents the real part of Z_0 . The dashed red line represents the imaginary part of Z_0	25
4.1	Original version of Menzel's antenna; $\epsilon_r = 2.33 - 0.0028$, $h = 0.0787cm$, $l = 19cm$, $w = 1.5cm$	26
4.2	(a) Two Dimension Color Figure of the field component E_y from the top view. Operation Frequency is 6Ghz. $\epsilon_r = 2.33 - 0.0028$, $h = 0.0787cm$, $l = 19cm$, $w = 1.5cm$. (b) Magnitude of the field component E_y along z-axis direction of the patch	27
4.3	(a) Menzel's antenna: Simulation Result E_{phi} far-field radiation pattern versus θ ; $\epsilon_r = 2.33 - 0.0028$, $h = 0.0787cm$, $l = 19cm$, $w = 1.5cm$. (b) Bandwidth of an leaky-wave antenna based on theory of the Transverse Resonance Method.	28
4.4	Full-width microstrip leaky wave antenna with two symmetrical feeds and two loads; $\epsilon_r = 2.33 - 0.0028$, $h = 0.0787cm$, $l = 19cm$, $w = 1.5cm$	29
4.5	Full-width: (a) Two-Dimension Color Figure of the field component E_y from the top view. Operation Frequency is 6Ghz. $\epsilon_r = 2.33 - 0.0028$, $h = 0.0787cm$, $l = 19cm$, $w = 1.5cm$. (b) Magnitude of the field component E_y along z-axis (length of the patch).	30
4.6	Fullwidth leaky-wave antenna Simulation: E_{phi} far-field radiation pattern versus θ ; $\epsilon_r = 2.33 - 0.0028$, $h = 0.0787cm$, $l = 19cm$, $w = 1.5cm$	31
4.7	Half-width microstrip leaky wave antenna with Single Feed and one load(50ohm); $\epsilon_r = 2.33 - 0.0028$, $h = 0.0787cm$, $l = 19cm$, $w = 0.75cm$	31
4.8	(a) Full-width: Two-Dimension Color Figure of the field component E_y . f=6Ghz. (b) Full-width: Magnitude of the field component E_y along z-axis (length of the patch). (c) Half-width: Two-Dimension Color Figure of the field component E_y . f=6Ghz. (d) Half-width: Magnitude of the field component E_y along z-axis (length of the patch).	32

4.9	Half-width Simulation: E_{phi} far-field radiation pattern of versus θ ; $\epsilon_r = 2.33 - 0.0028$, $h = 0.0787cm$, $l = 19cm$, $w = 0.75cm$	33
4.10	Comparison of Maximal Antenna Gain versus frequency of Menzel's, Full-width and Half-width antenna	34
4.11	The solid blue lines represent the theoretical normalized phase constant and attenuation constant based on the Transverse Resonance Method. The red stars represent the simulation results based on the Finite Element Method (FEM).	35
4.12	E_y field distribution:- simulation results of the fullwidth patch antenna with two symmetrical feeds structure compared with theoretical results. The stars represent the theoretical result and the solid lines represent the simulation result. $f = 6Ghz$	37
4.13	E_y field distribution:- simulation results of the fullwidth patch antenna with two symmetrical feeds structure compared with theoretical results. The stars represent the theoretical result and the solid lines represent the simulation result. $f = 7Ghz$	37
4.14	Comparing the Bandwidth of the microstrip line leaky wave antenna with different dielectric constant. $\epsilon_r = 2.33 - 0.0028$ and $\epsilon_r = 2.1$. .	39
4.15	Comparing the Bandwidth of the microstrip line leaky wave antenna with different dielectric constant. $\epsilon_r = 2.33 - 0.0028$ and $\epsilon_r = 1.9$. .	39
4.16	Comparing the Bandwidth of the microstrip line leaky wave antenna with different dielectric constant. $\epsilon_r = 2.33 - 0.0028$ and $\epsilon_r = 1.5$. .	40
4.17	Radiation pattern of this inhomogeneous leaky-wave antenna at $f=8Ghz$. $\epsilon_r = 2.33 - j0.0028$ and $\epsilon_r = 1.5$	41
4.18	Bandwith of this inhomogeneous leaky-wave antenna.	41
4.19	3-D view of an inhomogeneous substrate microstrip leaky wave antenna.	42
4.20	44
4.21	Comparison for Bandwidth of full-width microstrip leaky-wave antenna with inhomogeneous substrate leaky-wave antenna	44
4.22	Radiation pattern of the maximal gain and two patterns of 50% gain for the homogeneous Full-width Leaky-wave antenna.	45

4.23	Radiation pattern of the maximal gain and two patterns of 50% gain for the inhomogeneous Full-width Leaky-wave antenna.	46
4.24	Inhomogeneous substrate leaky-wave antenna (a)Bandwidth versus the length of the segment. (b)Bandwidth versus the relative length of segment w.r.t. the wavelength corresponding to an operation frequency of 10Ghz.	46

CHAPTER 1

INTRODUCTION

In conventional antennas, a heavy antenna rotating mechanism was necessary to scan beams but is very expensive and slow. Recently, printed leaky-wave antennas (LWAs) have attracted a lot of attention due to the advantages of broad VSWR (Voltage Standing Wave Ratio) bandwidth performance, their high relative directivity, and frequency scanning capabilities. Leaky-wave antennas are lightweight, easy to fabricate, and readily integrated into conventional millimeter-wave systems—properties that make leaky-wave antennas the subject of continuing interest today.

During the late 1970's, a paper presented by Ermert [3] concluded that a radiation region exists close to the cutoff frequency of higher modes for the microstrip line antenna (Fig 1.1). In Fig 1.1, EH_0 is the fundamental mode, and EH_1 and EH_2 are the next higher modes. In fact, if the operational frequency is below the cutoff frequency corresponding to these higher order modes, then the propagation constant is no longer purely real but is complex, representing the loss of power due to radiation as the wave propagates down the line. From the perspective of an integrated circuit, this leakage of radiation causes unwanted coupling, but in the desired characteristics from the perspective of antennas.

In 1979, Wolfgang Menzel presented a leaky-wave antenna by using an open microstrip line [1]. It was called Menzel's antenna later on. By exciting the first higher mode by a single asymmetrical feed structure the microstrip line radiated power into

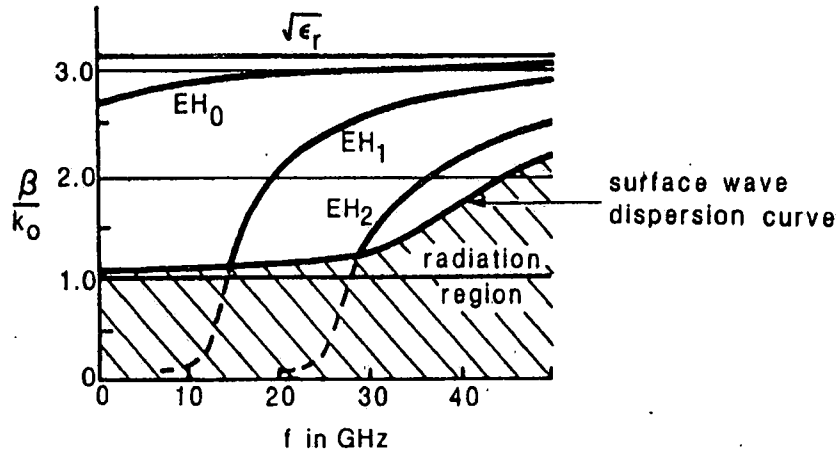


Figure 1.1: Normalized phase constant β/k_0 versus frequency f for the lowest mode and the first two higher modes in microstrip line with a top cover. The solid lines given by Ermert represent real wave numbers, whereas the dashed lines are corresponding to the real parts of the phase constant of the leaky mode solution in the radiation region. The dimensions of this microstrip line are width 3.00mm, dielectric layer thickness 0.635mm, $\epsilon_r = 9.80$, and the height of the top cover is 5 times the dielectric layer thickness.

space while the leaky wave propagated along the length of patch. During the 1980s, Arthur A. Oliner and K. S. Lee presented several papers about the leakage characteristics of higher modes on a microstrip line antenna[4][5] [6]. In his paper [6], Oliner provided two figures of the variations with frequency of the normalized phase constant β/k_0 and the normalized attenuation constant α/k_0 (Fig1.2 and 1.3). The two plots Oliner have shown in his paper were derived by the method of Steepest Descent Plane. These two results are quite crucial to us, because they specify the propagation characteristics of the higher modes for a given open microstrip line antenna. These results determine the cutoff frequencies of the higher order modes and also the achievable bandwidth.

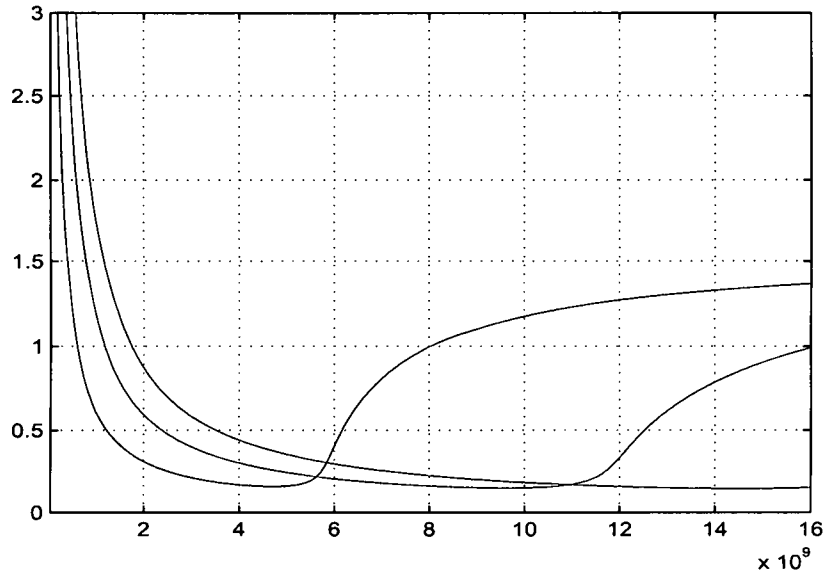


Figure 1.2: Normalized Phase constant β/k_0 versus frequency for the first three higher modes of open microstrip line.

Recently, Hong proposed a broadband leaky-wave antenna by tapering the patch width linearly [7] and a single-conductor strip leaky-wave antenna without the ground plane [8]. Chen reported a double-layer leaky-wave microstrip antenna [9]. Grbic presented a coplanar waveguide (CPW) based leaky wave antenna for Millimeter-Wave Applications [10]. Zelinski presented several microstrip leaky-wave antennas using first higher mode [2].

In chapter 2 of this thesis, we introduce some basic concepts of "leaky modes" (or "leakage phenomenon"). In Chapter 3 we present some theoretical discussion of complex characteristics of the leaky modes in an open microstrip line. By making use of the Transverse Resonance Method the complex propagation constants of the leaky modes were determined. These results are based on the reflection coefficient at the interface of a Parallel-Plate waveguide given by Chang and his co-authors [11][12] [13].

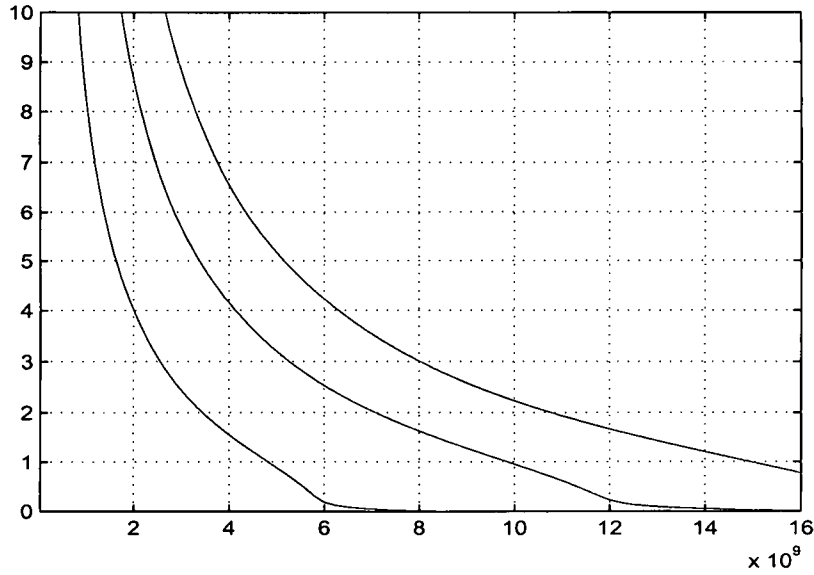


Figure 1.3: Normalized attenuation constant α/k_0 versus frequency for the first three higher modes of open microstrip line.

Chapter 3 also presents a discussion of the microstrip line modeled as two PEC walls at the top and bottom and symmetric impedance walls as the side walls. This model is used to determine the fields inside the waveguide which in turn are used to determine the driving point impedance, as also the wave impedance. In Chapter 4 we compare the theoretical values of the complex propagation constant with the results obtained using the Finite Element simulation (FE). It may be noted that the simulation is based on the Finite Element Boundary Integral code written by Professor Leo Kempel of the Michigan State University. In this chapter, we reviewed Menzel's antenna and then present two improved versions of Menzel's antenna: Full-width and Half-width leaky wave antennas.

CHAPTER 2

LEAKY WAVE PHENOMENON

2.1 Basic Definition

Surface waves, leaky waves and slot arrays, all of them come under the category of travelling waves.

1. Surface waves are usually purely bound waves and are slow waves. These radiate only at discontinuities, typically at the end of the structure.
2. Leaky waves are fast waves. A leaky-wave antenna is basically a waveguiding structure that possesses a mechanism that permits it to leak power all along its length. Typical waveguide modes are fast waves and can support leaky waves through long slots. However, many open dielectric waveguides typically have purely bounded slow waves as the dominant modes. These can not support leaky waves, unless properly designed asymmetries are introduced. These asymmetries must introduce new modes that correspond to fast waves, in order to support leaky modes. The asymmetries introduced may be such that the antenna is (nearly) uniform along its length or it is periodically modulated. The uniform leaky wave antenna radiates into the first quadrant, from nearly broadside (corresponding to the lower frequency of operation) to nearly endfire (corresponding to the highest frequency of operation).

The uniform leaky wave antennas can be either

- Single medium structure
- multiple medium structure

The multiple medium structure usually possess a fast wave ($\beta < k_0$) or a slow wave ($\beta > k_0$) region with a fast transition between these regions. $\beta = k_0$ corresponds to endfire and it is possible to get fairly close to endfire. Also, relatively small Δf can give significantly scan the main beam.

2.2 Introductory Principles of Leaky Wave

Let us consider a two-dimensional problem of an open microstrip line with $\frac{\partial}{\partial y} = 0$ and this approximation has its practical meaning. Suppose the right plane boundary of the patch of an open microstrip line or a waveguide is defined by the $x = 0$ plane Fig 2.1. We wish to support a leaky wave in the $x > 0$ region. For the purpose of

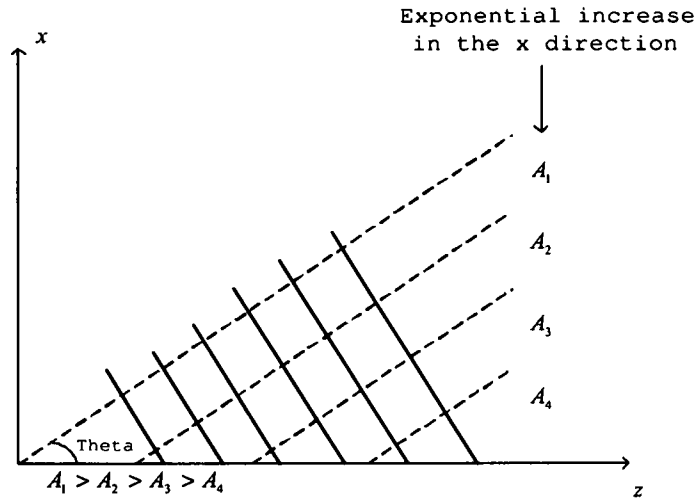


Figure 2.1: Two dimension figure for forward leaky wave

simplifying we assume that the dielectric or other guiding structure is located below $x = 0$ and that free space extends to infinity in the $+x$ direction. Then, a wave function satisfying the 2D wave equation is given by

$$u(x, z) = u_0 e^{-jk_z z} e^{-jk_x x}, \quad (2.1)$$

where k_z and k_x are the propagation constant along z direction and x direction. They could be complex numbers. That is

$$k_z = \beta_{zr} - j\alpha_z \text{ and } k_x = \beta_{xr} - j\alpha_x. \quad (2.2)$$

Thus, $u(x, z)$ may also be expressed as,

$$u(x, z) = u_0 e^{-j\vec{\beta} \cdot \vec{r}} e^{-j\vec{\alpha} \cdot \vec{r}} = u_0 e^{-\vec{\Gamma} \cdot \vec{r}}, \quad (2.3)$$

where $\vec{\Gamma} = \vec{\alpha} + j\vec{\beta}$; $\vec{\alpha} = \alpha_x \hat{a}_x + j\alpha_z \hat{a}_z$; $\vec{\beta} = \beta_{xr} \hat{a}_x + j\beta_{zr} \hat{a}_z$. However

$$k_z^2 + k_x^2 = k^2 = \omega^2 \mu \epsilon. \quad (2.4)$$

For our case, for $x > 0$, we have $\mu = \mu_0$, $\epsilon_r = \epsilon_0$ and $k_z^2 + k_x^2 = \omega^2 \mu_0 \epsilon_0$. Note that k_z must be the same for both $x > 0$ and $x < 0$ along propagation in the z direction. Equalizing the real and imaginary parts from (2.4), we get

$$\beta_{zr}^2 + \beta_{xr}^2 - (\alpha_x^2 + \alpha_z^2) = k^2 \quad (2.5)$$

and

$$\beta_{zr} \cdot \alpha_z + \beta_{xr} \cdot \alpha_x = 0. \quad (2.6)$$

From (2.6) we know, $\vec{\beta} \cdot \vec{\alpha} = 0$, which implies that the constant phase and constant amplitude planes are perpendicular to each other. Now, let us consider the following cases:

Case i) Trapped Surface Wave:-

The trapped surface wave propagates the finite amount of power along the surface without attenuation, and it decays exponentially in the transverse $+x$ direction. So of course, $\beta_{xr} = 0$; let $k_x = -j\alpha_x$; . Then for $x > 0$,

$$u(x, z) = u_0 e^{-j\vec{k}_z \cdot \vec{z}} \cdot e^{-j\alpha_x x}. \quad (2.7)$$

Because the wave decays exponentially in the transverse $+x$ direction., we must have $\alpha_x > 0$. Also, since $\beta_{xr} = 0$, considering(2.6) we derive $\beta_{zr}\alpha_z = 0$. Since $\beta_{zr} \neq 0$ (there would be no propagation otherwise), $\alpha_z = 0$! Then we have

$$\beta_{zr}^2 - \alpha_x^2 = k^2 = \omega^2 \mu_0 \epsilon_0. \quad (2.8)$$

Thus in this case $\beta_{zr} \geq k$. As a result, this "trapped surface wave" must be a Slow wave! Finally, as β_{zr} is increased from small values, surface wave modes begin to form for $\beta_{zr} = k$.

Case ii) Leaky waves:-

Now, let us consider the possibility of supporting "space waves" rather than surface waves radiating into the "forward" hemisphere. That is the wave which propagates in both the z - and x - directions. Therefore $\beta_{zr} > 0$ and $\beta_{xr} > 0$. The wave can only decay in the direction of propagation in the guide, namely z - direction, which means $\alpha_z > 0$. According to (2.6), with $\beta_{zr} > 0$ and $\beta_{xr} > 0$, when the condition $\alpha_z > 0$ is true, we derive $\alpha_x < 0$. As a result, this mode is an improper wave, ie, grows in the x - direction! Note that both k_z and k_x are complex, whereas for a Surface wave k_z is purely real and k_x is purely imaginary. As β_{zr} is decreased below k_0 (this is not a very precise statement), trapped surface wave modes can not exist but the leaky wave modes begin to form. The leaky waves radiate at an angle θ_c given by

$$\tan\theta = \frac{\beta_{xr}}{\beta_{zr}}, \quad (2.9)$$

or

$$\sin\theta = \frac{\beta_{xr}}{\sqrt{\beta_{xr}^2 + \beta_{zr}^2}} \quad (2.10)$$

CHAPTER 3

THEORETICAL ANALYSIS OF LEAKY WAVES IN MICROSTRIP

3.1 An Oblique Incident TEM Wave in a Parallel-plate Waveguide

Let us consider the problem of a parallel-plate waveguide or the parallel-plate waveguide model for an open microstrip line. A conducting plate of width 'w' is placed on the top of a grounded slab of thickness 'd'. The dielectric slab of the waveguide is assumed to be lossless, having a relative permittivity ϵ_r and permeability μ_r . A TEM wave of unit amplitude is incident obliquely onto the left substrate wall in the parallel plate region between the patch and the ground at an angle Φ with respect to the x axis (Fig3.1). At the boundary, the wave will be partially reflected by the substrate wall and partially radiate into the free space if the incident angle of the propagation wave Φ is set up to be greater than a critical angle. The part that radiates into the free space becomes the leaky wave.

Referring to Chang and Kuester's paper[12], let us define $k_{z_{nor}} = n \sin \Phi$, where $n = (\mu_r \epsilon_r)^{1/2}$, as the refractive index of the substrate. In fact, $k_{z_{nor}}$ is also the normalized propagation constant along the propagating direction z. And by making the approximation that there is no field changing between the patch and the ground because of the very thin thickness of the substrate, the propagation constant along y

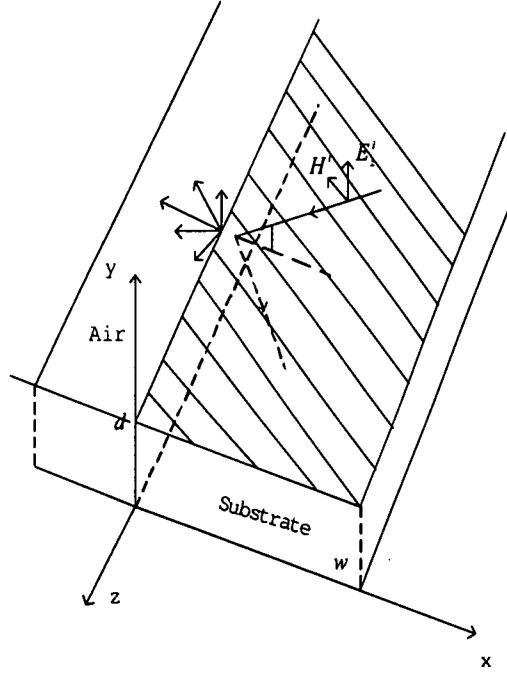


Figure 3.1: TEM wave incident onto the left boundary of a microstrip line or a dielectric filled parallel-plate waveguide.

axis is approximately equal to zero.

$$k_y = 0. \quad (3.1)$$

Therefore, the field components associated with this incident wave can be written as

$$\begin{aligned} E_y^i &= \exp \{ -jk_0[k_{z_{nor}}z - (n^2 - k_{z_{nor}}^2)^{1/2}x] \} \\ H_\Phi^i &= -(\mu_r\eta_0)^{-1}[\mathbf{a}_z(n^2 - k_{z_{nor}}^2)^{1/2} + \mathbf{a}_xk_{z_{nor}}] \cdot \exp \{ -jk_0[k_{z_{nor}}z - (n^2 - k_{z_{nor}}^2)^{1/2}x] \}, \end{aligned} \quad (3.2)$$

with a suppressed time factor of $\exp(j\omega t)$, $k_0 = \omega(\mu_0\epsilon_0)^{1/2}$ is the free space wave number, $\eta_0 = (\mu_0\epsilon_0)^{1/2} = 120\pi(\text{ohms})$ is the free space wave impedance, \mathbf{a}_z and \mathbf{a}_x are the unit vectors in the z and x directions. Without the y component, consequently the normalized propagation constant along x axis is calculated to be $(n^2 - k_{z_{nor}}^2)^{1/2}$. In the following sections, we will seek an explicit solution for $k_{z_{nor}}$, which is the

normalized propagation constant along direction of the length of patch, using the Transverse Resonance Method and perturbation techniques.

3.2 Tranverse Resonance Method

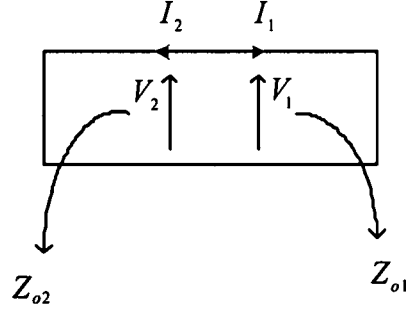


Figure 3.2: Transverse Section of waveguide or microstrip (Z_{01} and Z_{02} are the characteristic impedances).

First,

$$Z_{in,1} = \frac{V_1}{I_1}, \text{ and } Z_{in,2} = \frac{V_2}{I_2} = \frac{V_1}{-I_1} = -Z_{in,1}, \quad (3.3)$$

where $Z_{in,1}$ and $Z_{in,2}$ are the input impedances. $Z_{in,1}$ denotes the input impedance looking into the right from the middle of the cross section. $Z_{in,2}$ denotes the input impedance looking into the left from the middle. Their relation was given by (3.3).

$$Z_{in,1} = \frac{V_1}{I_1} = \frac{V_1^+ + V_1^-}{I_1^+ + I_1^-}, \quad (3.4)$$

where V^+ and I^+ are forward components, and V^- and I^- are backward components which are due to the reflected waves. The wave solution of a transmission line is the sum of forward and backward components.

$$I^+ = \frac{V_1^+}{Z_{01}}, \text{ and } I^- = -\frac{V_1^-}{Z_{01}}. \quad (3.5)$$

Substituting equation (3.5) into (3.4), and we get

$$Z_{in,1} = Z_{01} \frac{V_1^+ + V_1^-}{V_1^+ - V_1^-} = Z_{01} \left[\frac{1 + \Gamma_1(l_1)}{1 - \Gamma_1(l_1)} \right], \quad (3.6)$$

where $\Gamma_1(l_1) = \frac{E^r}{E^i} = \frac{V_1^-}{V_1^+}$ [14] is the reflection coefficient in the middle of the transverse section of the patch due to the wave reflected by the right-side boundary of this waveguide. In a similar manner

$$Z_{in,2} = Z_{02} \left[\frac{1 + \Gamma_2(l_2)}{1 - \Gamma_2(l_2)} \right], \quad (3.7)$$

where $\Gamma_2(l_2) = \frac{E^r}{E^i} = \frac{V_2^-}{V_2^+}$ is the reflection coefficient in the middle of the transverse section due to the wave reflected by the left-side boundary of this waveguide.

From (3.3) we know $Z_{in,2} = -Z_{in,1}$, which means that the input impedance at the middle point of the transverse section looking into the left is the negative value of input impedance looking into the right. Now use (3.6) and (3.7) to obtain

$$\begin{aligned} Z_{01} \left[\frac{1 + \Gamma_1(l_1)}{1 - \Gamma_1(l_1)} \right] &= Z_{02} \left[\frac{1 + \Gamma_2(l_2)}{1 - \Gamma_2(l_2)} \right] \\ (1 + \Gamma_1)(1 - \Gamma_2) &= -(1 - \Gamma_1)(1 + \Gamma_2) \\ 1 - \Gamma_2 + \Gamma_1 - \Gamma_1\Gamma_2 &= -(1 + \Gamma_2 - \Gamma_1 - \Gamma_1\Gamma_2) \\ 1 &= \Gamma_1\Gamma_2 \\ \Gamma_1 &= \frac{1}{\Gamma_2}, \end{aligned} \quad (3.8)$$

where Γ_1 is $\Gamma_1(l_1)$ and Γ_2 is $\Gamma_2(l_2)$. Note that $Z_{01} = Z_{02}$ because they both correspond to the wave impedance of the microstrip in the transverse direction.

Let Γ^b represent the reflection coefficient at the left or right of the transverse section of the parallel-plate waveguide. From [14][pp181,182], we learn that away from the boundary the reflection coefficient is related to the reflection coefficient at the boundary Γ^b and can be written as

$$\Gamma_1(l_1) = \Gamma(x = -l_1) = \frac{E^r(x)}{E^i(x)} \Big|_{x=-l_1} = \frac{\Gamma^b E_0 e^{+j\beta_1 x}}{E_0 e^{-j\beta_1 x}} \Big|_{x=-l_1} = \Gamma^b e^{-j2\beta_1 l_1}. \quad (3.9)$$

In a similar manner,

$$\Gamma_2(l_2) = \Gamma(x = l_2) = \frac{E^r(x)}{E^i(x)} \Big|_{x=l_2} = \frac{\Gamma^b E_0 e^{-j\beta_1 x}}{E_0 e^{+j\beta_1 x}} \Big|_{x=l_2} = \Gamma^b e^{-j2\beta_1 l_2}, \quad (3.10)$$

where l_1 and l_2 are positive distances measured from the boundary to the internal waveguide or microstrip. In our problem, $l_1 = l_2 = l = \frac{w}{2}$ and w is the width of the patch of the open microstrip line. β_1 is k_x the propagation constant along x-axis which is along the width of microstrip. In order to make the reader understand the formula easily, we keep the notation used in [14]. Thus we could obtain,

$$\Gamma_1(l_1) = \Gamma_2(l_2) = \Gamma = \Gamma^b e^{-j2k_x l}. \quad (3.11)$$

The reflection coefficient of the TEM wave at the boundary in this case can be expressed in the form $\Gamma^b(k_{znor}) = \exp[+j\chi(k_{znor})]$ so that its magnitude is unity [12]. From (3.8) we know $\Gamma_1(k_{znor})\Gamma_2(k_{znor}) = 1$. Thus

$$e^{-j4k_x l} e^{j2\chi(k_{znor})} = 1 = e^{j2\pi p}, p = 0, \pm 1, \pm 2, \dots \quad (3.12)$$

Therefore, we obtain

$$\begin{aligned} 2\chi(k_{znor}) - 4k_x l &= 0, \pm 2\pi, \pm 4\pi, \dots \\ \chi(k_{znor}) - 2k_x l &= 0, \pm \pi, \pm 2\pi, \pm 3\pi, \dots \\ \chi(k_{znor}) - 2k_x l &= \pm p\pi, \quad p = 0, 1, 2, 3, \dots \\ \chi(k_{znor}) - k_x w &= \pm p\pi, \quad p = 0, 1, 2, 3, \dots, \end{aligned} \quad (3.13)$$

where p denotes the mode number in x direction. This will be talked about later more detailly.

3.3 An Explicit Expression for the Propagation Constant of An Open Microstrip

In [12], the reflection coefficient $\Gamma_b(k_{znor})$ of the wave at the interface of the strip is found to be

$$\Gamma^b(k_{znor}) = \exp[+j\chi(k_{znor})], \quad (3.14)$$

where

$$\chi(k_{znor}) = 2 \tan^{-1} \left(\frac{k_{znor}}{\sqrt{n^2 - k_{znor}^2}} \tanh \Delta \right) - f_e(-\sqrt{n^2 - k_{znor}^2}), \quad (3.15)$$

where $n = \sqrt{\epsilon_r \mu_r}$ and

$$\Delta \cong \frac{k_{znor} k_0 d}{\pi} \left\{ \left(\frac{1}{\epsilon_r} - \mu_r \right) [\ln(\sqrt{k_{znor}^2 - 1} k_0 d) + \gamma - 1] + 2Q_0(-\delta_e) - 2Q_0(\delta_\mu) \right\}, \quad (3.16)$$

$$f_e(-\sqrt{n^2 - k_{znor}^2}) \cong -\frac{2\sqrt{n^2 - k_{znor}^2} k_0 d}{\pi} \cdot \left\{ \frac{1}{\epsilon_r} [\ln(\sqrt{k_{znor}^2 - 1} k_0 d) + \gamma - 1] + 2Q_0(-\delta_e) - \ln 2\pi \right\}. \quad (3.17)$$

Note that here n is not the one used in (3.13).

Assuming $k_0 d$ is extremely small, and in addition assuming that $|k_0 d / \sqrt{n^2 - k_{znor}^2}|$ and $|k_0 d / k_{znor}|$ are small, we obtain

$$\chi(k_{znor}; k_0) \cong \frac{2k_{znor}}{\sqrt{n^2 - k_{znor}^2}} \Delta - f_e(-\sqrt{n^2 - k_{znor}^2}). \quad (3.18)$$

Substituting (3.17) into (3.18) and combining with (3.16), we derive

$$\chi(k_{znor}; k_0) \cong \frac{2k_0 d}{\pi \sqrt{n^2 - k_{znor}^2}} G(k_{znor}; k_0), \quad (3.19)$$

where

$$G(k_{znor}; k_0) = (1 - k_{znor}^2) \mu_r [\ln(\sqrt{k_{znor}^2 - 1} k_0 d) + \gamma - 1] + n^2 [2Q_0(-\delta_e) - \ln 2\pi] - k_{znor}^2 [2Q_0(\delta_\mu) - \ln 2\pi], \quad (3.20)$$

where

$$\begin{aligned} Q_0(z) &= \frac{z}{1-z} Q_1(z) \\ Q_0(-\delta_e) &= \frac{-\delta_e}{1+\delta_e} Q_1(-\delta_e) \\ Q_0(\delta_\mu) &= \frac{\delta_\mu}{1-\delta_\mu} Q_1(\delta_\mu), \end{aligned} \quad (3.21)$$

and δ_e and δ_μ are given as

$$\delta_e = \frac{\epsilon_r - 1}{\epsilon_r + 1}, \text{ and } \delta_\mu = \frac{\mu_r - 1}{\mu_r + 1}. \quad (3.22)$$

Substituting (3.22) back into (3.21) and solving for $Q_0(-\delta_\epsilon)$ and $Q_0(\delta_\mu)$, we obtain

$$Q_1(z) = \sum_{m=1}^{\infty} z^m \ln \left(\frac{m+1}{m} \right). \quad (3.23)$$

The function Q_1 converges more quickly than Q_0 , so here we choose Q_1 instead of function Q_0 . Since this Q_1 has the quick convergent characteristics, instead of making sum infinite terms we could just choose seven terms.

So far we have obtained a expression for $\chi(k_{znor}; k_0)$ in terms of the known variables. In last section, we learned that (3.13)

$$\begin{aligned} \chi(k_{znor}) - k_x w &= \pm p\pi, \quad p = 0, 1, 2, 3, \dots \\ \chi(k_{znor}) - k_0 w \sqrt{n^2 - k_{znor}^2} &= -p\pi, \quad p = 0, 1, 2, 3, \dots \end{aligned} \quad (3.24)$$

Substituting (3.19) right into (3.24) and solving for $\sqrt{n^2 - k_{znor}^2}$ as

$$\sqrt{n^2 - k_{znor}^2} = \frac{p\pi}{k_0 w} + \frac{1}{2} \left[\sqrt{\left(\frac{p\pi}{k_0 w} \right)^2 + 8 \frac{d}{\pi w} G(k_{znor}; k_0)} - \frac{p\pi}{k_0 w} \right]. \quad (3.25)$$

Then take the square on both sides and solve for k_{znor}^2 [13]

$$k_{znor}^2 = n^2 - \left\{ \frac{1}{2} \left(\frac{p\pi}{k_0 w} \right) \left[\sqrt{\left(\frac{p\pi}{k_0 w} \right)^2 + 8 \frac{d}{\pi w} G(k_{znor}; k_0)} + \frac{p\pi}{k_0 w} \right] + \frac{2d}{\pi w} G(k_{znor}; k_0) \right\}. \quad (3.26)$$

We notice that (3.26) is still an implicit equation, but an explicit solution for k_{znor} may be able to be obtained using pertubation techniques [13]

$$k_{znor} = n_{eff} \cong \begin{cases} n - \frac{d}{\pi n w} G(k_{znor}; k_0), & (p = 0) \\ \sqrt{k_{znorp}^2 - \frac{4d}{\pi w} G(k_{znorp}; k_0)}, & (p > 0) \end{cases} \quad (3.27)$$

where

$$k_{znorp} = \left[n^2 - \left(\frac{p\pi}{k_0 w} \right)^2 \right]^{1/2}, \quad (3.28)$$

given by [13] and function $G(k_{znorp}; k_0)$ was given by equation (3.20). p is the mode number of x direction. $p = 0$ denotes the fundamental mode which is the TEM

dominant mode and $p = 1, 2, 3, \dots$ denotes the first higher mode, the second higher mode and the third higher mode and so on. Note that $k_0 = 2\pi f(\mu_r \epsilon_r)^{1/2}$, where f is the operation frequency for the microstrip leaky wave antenna.

3.4 Leaky Modes on Microstrip Line Antenna

With the explicit expression for the propagation constant, all the properties of leakage from the higher modes are readily to obtain and analyze. First, the radiation region of those higher modes becomes clear to us. Those information is very helpful and significant for us to analyze and design a leaky-wave microstrip antenna. A matlab code based on the Transverse Resonance Method was developed for calculating the propagation constant along the microstrip line. Figure 3.3 plots the normalized

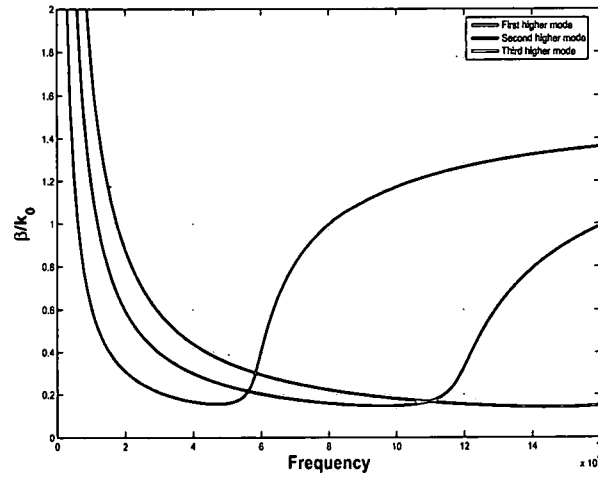


Figure 3.3: Normalized phase constant β/k_0 versus frequency for the first three higher modes of an open microstrip line. The dimensions of our microstrip line are thickness of the substrate $0.787mm$, the patch width $15mm$, dielectric constant $\epsilon_r = 2.33$.

phase constant versus frequency and fig3.4 plots the normalized attenuation constant versus frequency for a specific microstrip leaky wave antenna.

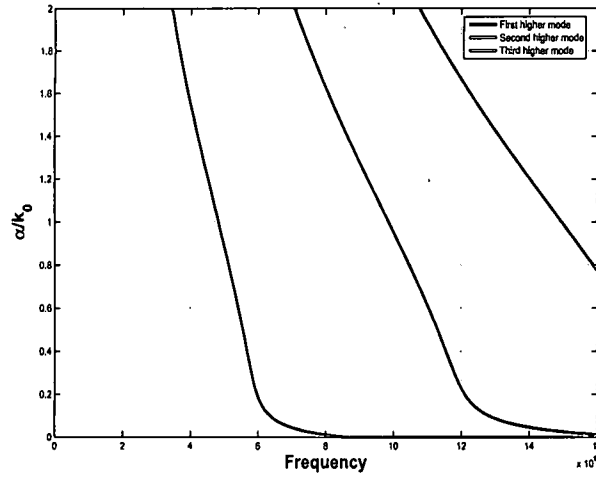


Figure 3.4: Normalized phase constant α/k_0 versus frequency for the first three higher modes of an open microstrip line. The dimensions of our microstrip line are thickness of the substrate $0.787mm$, the patch width $15mm$, dielectric constant $\epsilon_r = 2.33$.

The attenuation constant is zero when the operation frequency is above the cutoff frequency. For this configuration of microstrip leaky wave antenna, the cutoff frequency is around 8GHz. It shows that above that cutoff frequency the propagation constant is purely real so the microstrip line supports only a trapped surface wave but not leaky wave. It may be noted that at cut-off the relative phase constant is equal to unity and the radiation maximum occurs near end-fire. In the radiation region of this microstrip leaky wave antenna while k_z/k_0 is increasing from 0 to 1, the main beam sweeps from broadside to endfire.

From the information of propagation constant we calculated by the Transverse Resonance Method, the bandwidth of a microstrip line leaky-wave antenna can also be defined. Figure 3.5 shows the bandwidth of a leaky wave antenna. The lower frequency of the bandwidth is defined by the cross point of the normalized phase

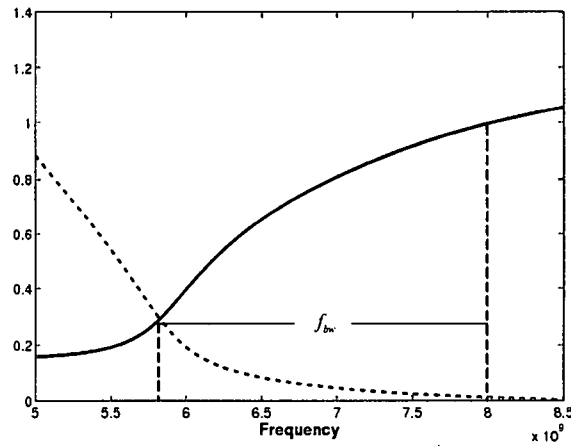


Figure 3.5: Bandwidth of microstrip line leaky-wave antenna by the Transverse Resonance Method.

constant with the normalized attenuation constant. The higher frequency of the bandwidth is defined by the point the normalized phase constant reached 1.

3.5 Driving Point Impedance of the First Higher Mode in the Open Microstrip Line

3.5.1 Fields and Modes in the Open Microstrip Line

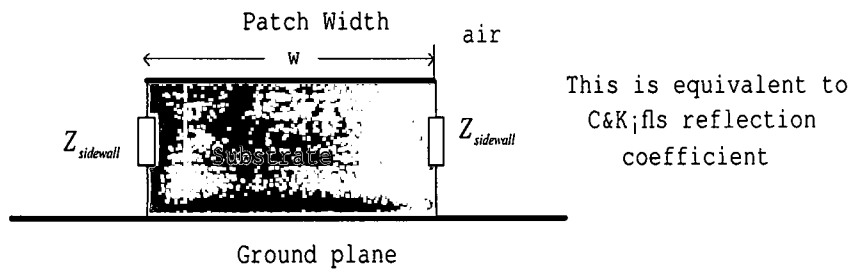


Figure 3.6: Transverse section of an open microstrip line

Both LSM^y and LSE^y can be existed in the microstrip line. For the LSM^y or TM^y mode, the field components are given as following

$$\begin{aligned} E_x &= \frac{1}{j\omega\mu\epsilon} \frac{\partial^2 A_y}{\partial x \partial y} & H_x &= -\frac{1}{\mu} \frac{\partial A_y}{\partial z} \\ E_y &= \frac{1}{j\omega\mu\epsilon} \left(\frac{\partial^2}{\partial y^2} + k^2 \right) A_y & H_y &= 0 \\ E_z &= \frac{1}{j\omega\mu\epsilon} \frac{\partial^2 A_y}{\partial y \partial z} & H_z &= \frac{1}{\mu} \frac{\partial A_y}{\partial x}, \end{aligned} \quad (3.29)$$

where A_y is the scalar potential function and for a $+z$ traveling waves, A_y is given by the expression

$$A_y = [C_1 \cos(k_x x) + D_1 \sin(k_x x)] [C_2 \cos(k_y y) + D_2 \sin(k_y y)] A_3 e^{-jk_z z}, \quad (3.30)$$

where

$$k_x^2 + k_y^2 + k_z^2 = k^2 = \omega^2 \mu \epsilon. \quad (3.31)$$

Substituting (3.30) into (3.29), we can write the x component of the electric field as

$$E_x = \frac{1}{j\omega\mu\epsilon} [-C_1 k_x \sin(k_x x) + D_1 k_x \cos(k_x x)] [-C_2 k_y \sin(k_y y) + D_2 k_y \cos(k_y y)] A_3 e^{-jk_z z}. \quad (3.32)$$

Satisfying the two boundary conditions along y direction on the metal plates we have that

- At $y = 0$, $E_x = 0 \Rightarrow D_2 = 0$
- At $y = d$, $E_x = 0 \Rightarrow k_y d = n\pi \Rightarrow k_y = n\pi/d$

Now substituting $D_2 = 0$ and $k_y = n\pi/d$ into (3.30) it reduces to

$$A_y = [C_1 \cos(k_x x) + D_1 \sin(k_x x)] C_2 A_3 \cos\left(\frac{n\pi}{d} y\right) e^{-jk_z z}, \quad (3.33)$$

where the first term gives the even mode and the second term gives the odd mode.

For the LSE^y or TE^y mode, the field components are given as following

$$\begin{aligned} E_x &= \frac{1}{\epsilon} \frac{\partial F_y}{\partial z} & H_x &= \frac{1}{j\omega\mu\epsilon} \frac{\partial^2 F_y}{\partial x \partial y} \\ E_y &= 0 & H_y &= \frac{1}{j\omega\mu\epsilon} \left(\frac{\partial^2}{\partial y^2} + k^2 \right) F_y \\ E_z &= -\frac{1}{\epsilon} \frac{\partial F_y}{\partial x} & H_z &= \frac{1}{j\omega\mu\epsilon} \frac{\partial^2 F_y}{\partial y \partial z}, \end{aligned} \quad (3.34)$$

$$F_y = (C_1 \cos(k_x x) + D_1 \sin(k_x x))(C_2 \cos(k_y y) + D_2 \sin(k_y y)) A_3 e^{-jk_z z}, \quad (3.35)$$

$$E_x = \frac{(-jk_z)}{\epsilon} (C_1 \cos(k_x x) + D_1 \sin(k_x x))(C_2 \cos(k_y y) + D_2 \sin(k_y y)) A_3 e^{-jk_z z}. \quad (3.36)$$

In the similar manner, satisfying the boundary conditions along y direction we have

- At $y = 0$, $E_x = 0 \Rightarrow C_2 = 0$.
- At $y = d$, $E_x = 0 \Rightarrow k_y d = n\pi \Rightarrow k_y = n\pi/d$.

Now (3.35) reduces to

$$F_y = (C_1 \cos(k_x x) + D_1 \sin(k_x x)) D_2 A_3 \sin\left(\frac{n\pi}{d} y\right) e^{-jk_z z}, \quad (3.37)$$

where the first term gives the odd mode and the second term gives the even mode.

Let us examine the modes which could exist in the microstrip line. We learned that both LSM^y and LSE^y mode can exist in the microstrip line. Suppose the modes are denoted by EH_{mn} where m denotes the mode number along x direction and n denotes the mode number along y direction. Therefore the lowest mode which is the fundamental mode can be denoted as EH_{00} according to the context. Noticing $m = 0$ and $n = 0$ we have the propagation constant $k_x = 0$ and $k_y = 0$ respectively, which means that there are no field changes in the transverse directions. The first higher mode is defined by $m = 1$ which is the mode number in the x-axis. How about the mode number in the other direction of the transverse section for the first higher mode? We know in the region between the patch and the ground plane, there is very

little change for the field with respect to y direction. Thus according to the analysis given above

$$k_y = 0 \text{ or } n = 0. \quad (3.38)$$

Therefore, we conclude that EH_{10} can represent the first higher mode we have talked about in the thesis. Now let us reexamine the scalar potential F_y of the LSE^y mode. If $k_y = 0$ then we will have $F_y = 0$ and it means that there will be no LSE^y component for the first higher mode! Hence, the first higher mode consists of only LSM^y mode. In Ermert's Paper [3], the first higher mode is denoted as EH_1 , and in the case of the covered microstrip line he divided the microstrip cross section into 4 regions. For each region of the microstrip cross section, the complete set of wave functions including both LSM^y mode and LSE^y mode was considered. In our work, only the region between the patch and the ground plane is considered. We satisfies the boundary conditions on the upper and lower PEC and we use the sidewall impedance to satisfy the other two boudary conditions which can also be analyzed by Chang & Kuester's approximation of reflection coefficient. Comparing with his method, our method not only reduces the work but also gives people more clear explanation of the field and mode analysis for those higher modes in the microstip line with a thin substrate thickness.

3.5.2 Driving Point Impedance of the First Higher Mode

Now let us derive driving point impedance of the first higher mode. Substituting (3.38) into (3.33) we derive

$$A_y = A_1 \sin(k_x x) e^{-jk_z z}. \quad (3.39)$$

Since $m = 1$ corresponds to the odd mode, we only take the \sin function for the LSM^y mode Thus according to (3.29) the field component E_y and H_x for this LSM_1^y

mode would be

$$\begin{aligned} E_y &= \frac{1}{j\omega\mu\epsilon} \left(\frac{\partial^2}{\partial y^2} + k^2 \right) A_y \\ &= \frac{k^2}{j\omega\mu\epsilon} \cdot A_1 \sin(k_x x) e^{-jk_z z}, \end{aligned} \quad (3.40)$$

and

$$H_x = -\frac{1}{\mu} \frac{\partial A_y}{\partial z} = -\frac{1}{\mu} (-jk_z) A_1 \sin(k_x x) e^{-jk_z z}. \quad (3.41)$$

The wave impedance along z direction is given by

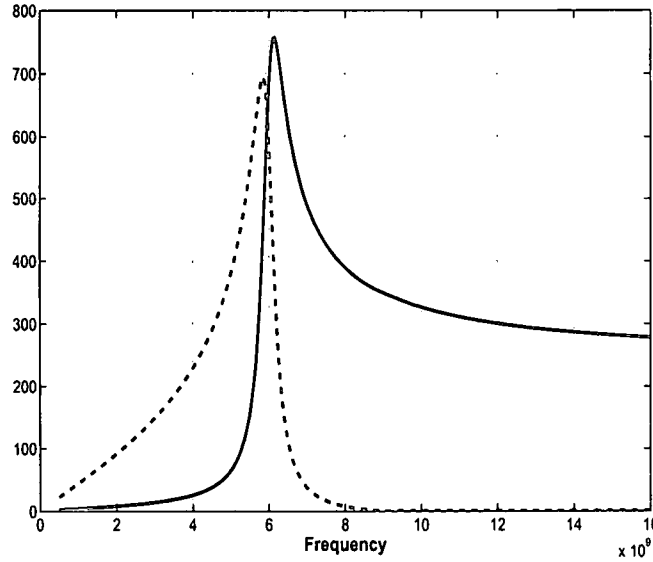


Figure 3.7: Analytical Results for the Driving Point Impedance for the first higher mode in z direction. The blue line represents the real part of Z_z . The dashed red line represents the imaginary part of Z_z .

$$Z_z = -\frac{E_y}{H_x} = -\frac{k^2}{j\omega\mu\epsilon} \frac{j k_z}{\mu} = -\frac{\mu k^2}{j\omega\mu\epsilon \cdot j k_z} = \frac{k^2}{\omega\epsilon k_z}. \quad (3.42)$$

Substituting $k^2 = \omega^2\mu\epsilon$ into (3.42) we can rewrite (3.42) as

$$Z_z = \frac{\omega\mu}{k_z} = \frac{\omega\sqrt{\mu}\sqrt{\mu}\sqrt{\frac{\epsilon}{\epsilon}}}{jk_z} = \frac{\eta}{\left(\frac{k_z}{k}\right)}. \quad (3.43)$$

Function (3.43) is an expression of the wave impedance for the first higher mode. From that, we can continue to derive the expression of the driving point impedance.

$$\begin{aligned} E_y &= \frac{k^2}{j\omega\mu\epsilon} \cdot A_1 \sin(k_x x) e^{-jk_z z} \\ H_x &= -\frac{1}{\mu} (-jk_z) A_1 \sin(k_x x) e^{-jk_z z}. \end{aligned} \quad (3.44)$$

Consider the microstrip line as a model of parallel-plate waveguide. The voltage between the two parallel plates is given by the expression

$$\begin{aligned} V &= - \int_{y=0}^d \vec{E}_y dy \\ &= - \int_{y=0}^d \frac{k^2}{j\omega\mu\epsilon} \cdot A_1 \sin(k_x x) e^{-jk_z z} dy \\ &= -E_y d. \end{aligned} \quad (3.45)$$

The current flowing on the plate is given by the expression

$$\begin{aligned} I &= \int_{x=0}^w \vec{J}_s \cdot \hat{z} dx = \int_{x=0}^w (-\hat{y} \times \vec{H}) \cdot \hat{z} dx = \int_{x=0}^w H_x dx \\ &= \int_{x=0}^w -\frac{1}{\mu} (-jk_z) A_1 \sin(k_x x) e^{-jk_z z} dx \\ &= -\frac{1}{\mu} (-jk_z) A_1 e^{-jk_z z} \int_{x=0}^w \sin(k_x x) dx \\ &= -\frac{1}{\mu} (-jk_z) A_1 e^{-jk_z z} \cdot \frac{1}{k_x} [\cos(k_x x)] \Big|_{x=0}^{x=w} \\ &= -\frac{1}{\mu} (-jk_z) A_1 e^{-jk_z z} \cdot \frac{1}{k_x} [1 - \cos(k_x w)] \\ &= \frac{H_x}{\sin(k_x x)} \cdot \frac{1}{k_x} [1 - \cos(k_x w)]. \end{aligned} \quad (3.46)$$

Therefore, the driving point impedance of the first higher mode in the open microstrip line is derived as following

$$\begin{aligned} Z_0 &= \frac{V}{I} = \frac{-E_y \cdot d}{H_x} \cdot \frac{\sin(k_x x) k_x}{1 - \cos(k_x w)} \\ &= \frac{-E_y}{H_x} \cdot \frac{d \sin(k_x x) k_x}{1 - \cos(k_x w)} \\ &= Z_z \cdot \frac{d \sin(k_x x) k_x}{1 - \cos(k_x w)}. \end{aligned} \quad (3.47)$$

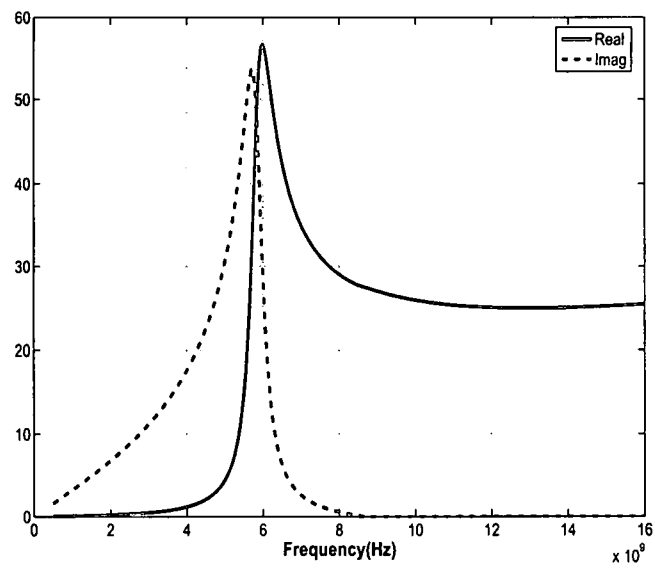


Figure 3.8: Analytical Results for the driving point Impedance for the first higher mode in z direction. The blue line represents the real part of Z_0 . The dashed red line represents the imaginary part of Z_0 .

CHAPTER 4

RESULTS: SIMULATION

4.1 Menzel's Antenna

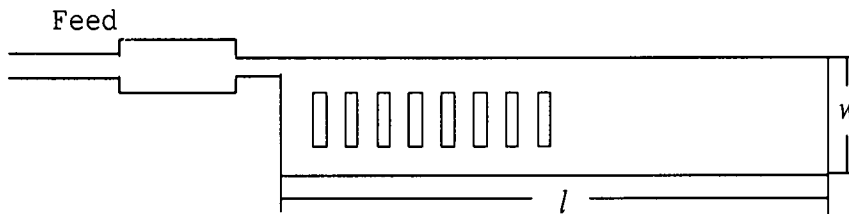


Figure 4.1: Original version of Menzel's antenna; $\epsilon_r = 2.33 - 0.0028$, $h = 0.0787cm$, $l = 19cm$, $w = 1.5cm$

In 1979, Menzel proposed a travelling wave antenna based on the open microstrip line [1]. It is the earliest microstrip leaky-wave antenna with exciting the first higher mode and subsequently investigated by a lot people [7] [15]. However there are many shortcomings of menzel's antenna for example the dominant mode still existing, back-lobes. In this chapter, we will investigate the original menzel's antenna once again and introduce two improved version of menzel's antenna.

The original version of Menzel's antenna Fig4.1 is fed asymmetrically by an single feeding structure It has several slots cut in the middle and along the patch. Since the

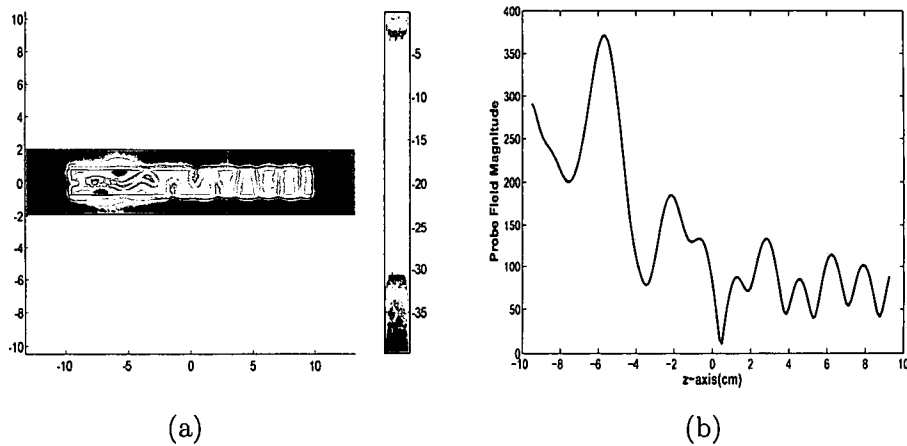
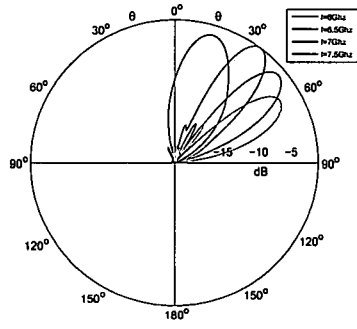


Figure 4.2: (a) Two Dimension Color Figure of the field component E_y from the top view. Operation Frequency is 6Ghz. $\epsilon_r = 2.33 - 0.0028$, $h = 0.0787cm$, $l = 19cm$, $w = 1.5cm$. (b) Magnitude of the field component E_y along z-axis direction of the patch

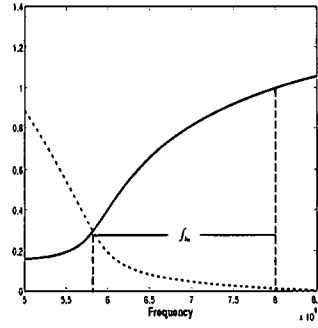
dominant mode has a maximum magnitude in the middle of the patch, the slots cut in the middle the patch is intended to suppress the dominant mode which supports a trapped surface wave. However the dominant mode is not eliminated completely by the slots and reflected at the end the patch (See Figure 4.2(a)(b)).

Thus the power did not radiate into space completely. Figure 4.2(a) shows a two-dimension color figure of the field distribution of E_y on the surface of the whole cavity. The slots do suppress the dominant mode somehow but at other segments of the patch where no slots were cut the dominant mode begin to appear and affect the behavior of the antenna. We can clearly see from figure 4.2(a) the presence of standing waves, suggesting that not all the power in the first higher order mode is radiated. It is also clear that the slot in the line line fail to suppress the fundamental mode completely.

Figure 4.2(b) shows the field component E_y versus z-axis (the direction of length of the patch). We know that if there is only the first higher mode existing in microstrip



(a)



(b)

Figure 4.3: (a) Menzel's antenna: Simulation Result E_{phi} far-field radiation pattern versus θ ; $\epsilon_r = 2.33 - 0.0028$, $h = 0.0787cm$, $l = 19cm$, $w = 1.5cm$. (b) Bandwidth of an leaky-wave antenna based on theory of the Transverse Resonance Method.

line the magnitude of E_y should be an exponential function. But clearly figure 4.2(b) does not show an exponential function, therefore for the menzel's antenna there are other modes besides the first higher mode existing in the microstrip line. The farfield radiation pattern and the antenna gain is shown in figure 4.3(a). The bandwidth of an leaky-wave antenna is normally defined as in figure 4.3(b). The lower frequency of the bandwidth is defined by the point of intersection of the normalized phase constant with the normalized attenuation constant. The higher frequency of the bandwidth is defined by the normalized phase constant equals 1. At the lower frequency, the main beam should correspond to broadside and at higher frequency the main beam is near endfire. In practice, when the normalized phase constant increases over 1 the leaky wave will be no longer exist, as the attenuation constant is zero and the wave becomes a trapped surface wave. In figure 4.3(a) the operational frequency varies from 5.9GHz up to 7.5GHz. However the bandwidth which is defined in figure 4.3(b) is much larger

than that range(5.9Ghz to 7.5Ghz). Those frequencies which are not in this range really have very low antenna gain and much wider beam.

4.1.1 Full-width Microstrip Line Leaky Wave Antenna with Two Symmetrical Feeds

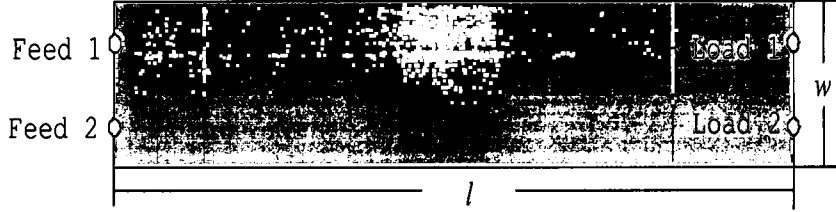


Figure 4.4: Full-width microstrip leaky wave antenna with two symmetrical feeds and two loads; $\epsilon_r = 2.33 - 0.0028$, $h = 0.0787cm$, $l = 19cm$, $w = 1.5cm$.

From last section, we learned that Menzel's antenna could not suppress the dominant mode completely and the dominant mode will influence the characteristic of leakage and add a negative effect to the leaky wave antenna's radiation pattern. In order to suppress the dominant mode completely, in this section we use a two-feed symmetrical feeding structure for exciting the first higher mode and at the same time suppressing the dominant mode (figure 4.4).

Both of the two feeds have the magnitude equal to 1.0 but one of the two feeds has a **0 degree** phase, the other phase is **180 degree**. It is known that the dominant mode has the maximum for field component E_y in the middle of the patch. With this two symmetrical feeds, we could artificially force the field component E_y to be zero in the middle of the patch so that the dominant mode gets suppressed. From figure 4.5(a) we could see that in the middle of the patch field component E_y is equal to zero and at other positions E_y attenuates along z-axis. Figure 4.5 plots the magnitude

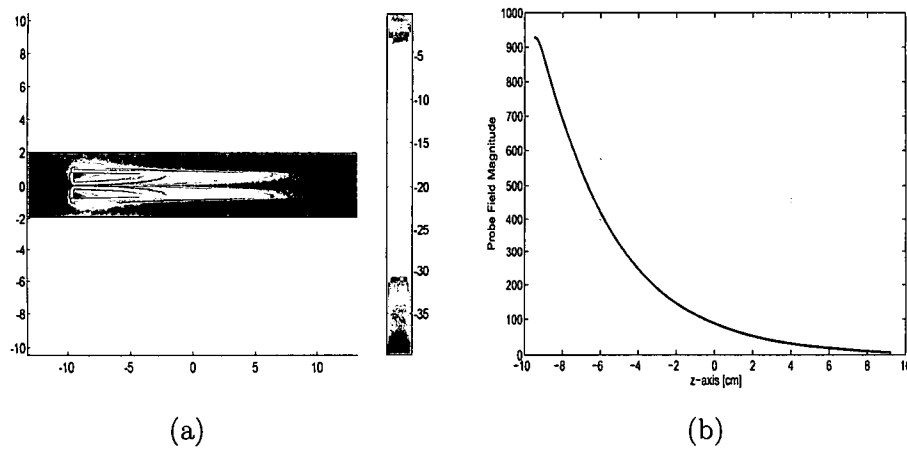


Figure 4.5: Full-width: (a) Two-Dimension Color Figure of the field component E_y from the top view. Operation Frequency is 6Ghz. $\epsilon_r = 2.33 - 0.0028$, $h = 0.0787\text{cm}$, $l = 19\text{cm}$, $w = 1.5\text{cm}$. (b) Magnitude of the field component E_y along z -axis (length of the patch).

of E_y from the data of a line of probes. It shows the magnitude of E_y exponentially attenuates along z -axis. It is known that the magnitude of the leaky mode's field is an exponential function so the dominant mode here is totally eliminated. Therefore, with this two symmetrical feeds only the first higher mode can exist in the microstrip line.

The radiation pattern of the fullwidth microstrip leaky wave antenna is shown in figure 4.6. The frequency varies from 5.7Ghz up to 8Ghz and the main beam also sweeps from broadside to endfire. Comparing the fullwidth antenna's radiation pattern with the pattern of Menzel's antenna (figure 4.3), the bandwidth of the fullwidth antenna from 5.7Ghz up to 8Ghz is wider than Menzel's and the antenna gain of the fullwidth antenna is twice as Menzel's antenna. In conclusion, with suppressing the dominant mode, we increase the the antenna's gain and make the bandwidth wider.

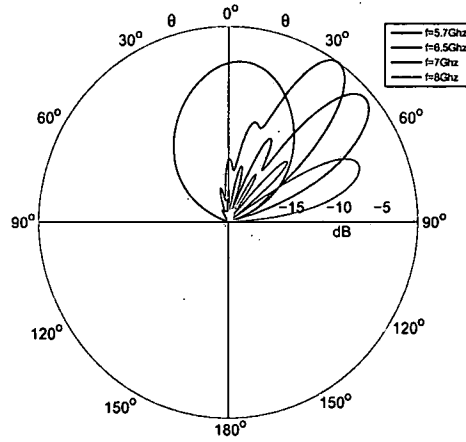


Figure 4.6: Fullwidth leaky-wave antenna Simulation: E_{phi} far-field radiation pattern versus θ ; $\epsilon_r = 2.33 - 0.0028$, $h = 0.0787\text{cm}$, $l = 19\text{cm}$, $w = 1.5\text{cm}$.

4.1.2 Half Width Microstrip Line Leaky Wave Antenna with Single Feed

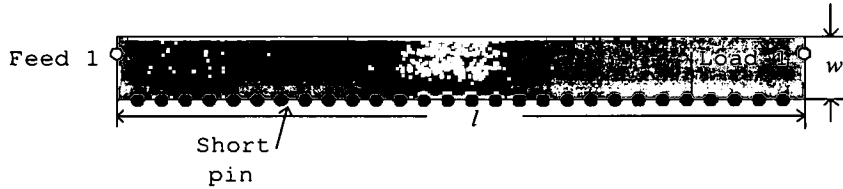


Figure 4.7: Half-width microstrip leaky wave antenna with Single Feed and one load(50ohm); $\epsilon_r = 2.33 - 0.0028$, $h = 0.0787\text{cm}$, $l = 19\text{cm}$, $w = 0.75\text{cm}$.

The two-feeds symmetrical feeding structure with one feed's phase being the negative value of the other's is able to suppress the dominant mode completely. However there is another method we might consider here for eliminating the dominant mode but at the same time exciting the first higher mode. In figure4.7, it shows a half-width

patch leaky-wave antenna($w = 0.75\text{cm}$) with a single feeding structure[2][16]. The width used for this patch antenna is half of the full-width patch.

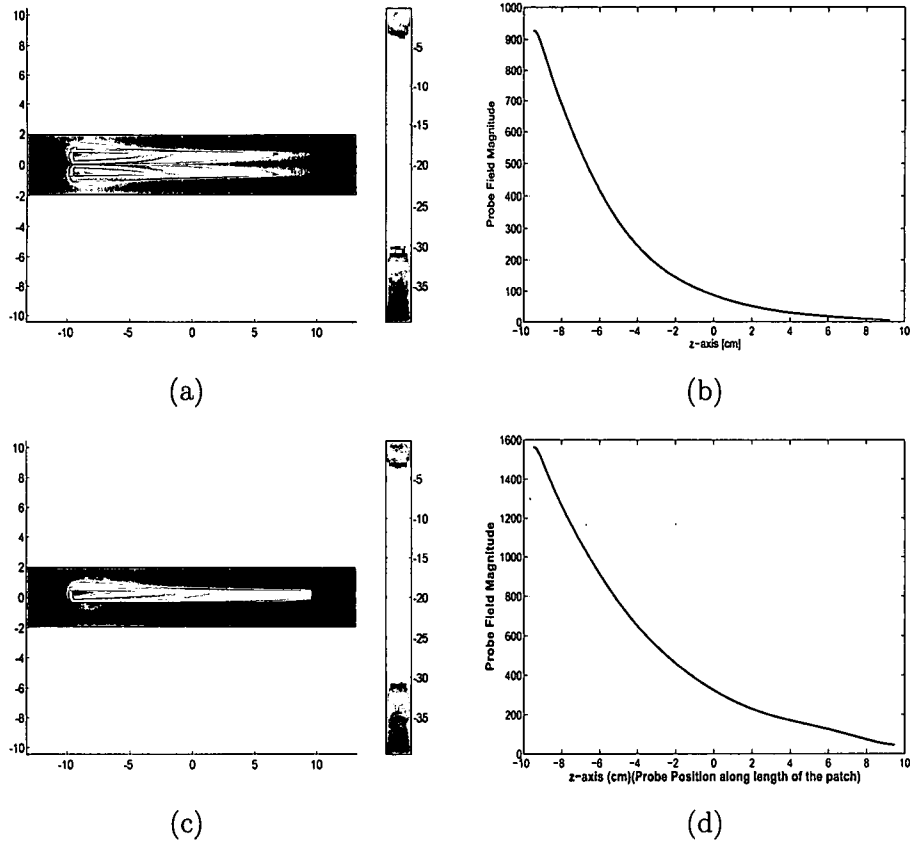


Figure 4.8: (a)Full-width: Two-Dimension Color Figure of the field component E_y . $f=6\text{GHz}$. (b)Full-width: Magnitude of the field component E_y along z -axis (length of the patch). (c)Half-width: Two-Dimension Color Figure of the field component E_y . $f=6\text{GHz}$. (d)Half-width: Magnitude of the field component E_y along z -axis (length of the patch).

In fact the short pins behave like mirror in the middle of the patch. One can imagine that there is another half of the patch existing below the short pins due to the mirror effect. If we combine the physically existed half-patch and the imaginary half-patch together, they will comprise the full-width microstrip patch antenna discussed

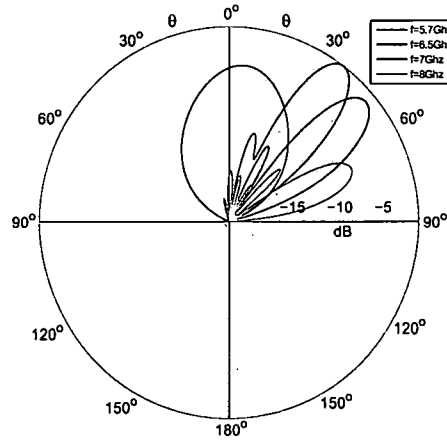


Figure 4.9: Half-width Simulation: E_{phi} far-field radiation pattern of versus θ ; $\epsilon_r = 2.33 - 0.0028$, $h = 0.0787cm$, $l = 19cm$, $w = 0.75cm$.

in the last section. Another way to understand how the half-width leaky wave antenna eliminates the dominant mode is to recognize that the short pins make the field component E_y to be zero in the middle of the patch so that the dominant mode is suppressed completely. And at the same time the single feed is able to excite the first higher mode.

The radiation pattern of this half-width microstrip line leaky wave antenna is shown in figure 4.9. While the frequency is increasing from 5.7Ghz to 8Ghz the beam direction also switches from broadside to endfire.

4.1.3 Bandwidth

The bandwidth of an antenna is defined as "the range of frequencies within which the performance of the antenna, with respect to some characteristic, conforms to a specified standard." [17][pp63]. The bandwidth can be considered to be range of frequencies, on either side of a center frequency , where the antenna characteristics

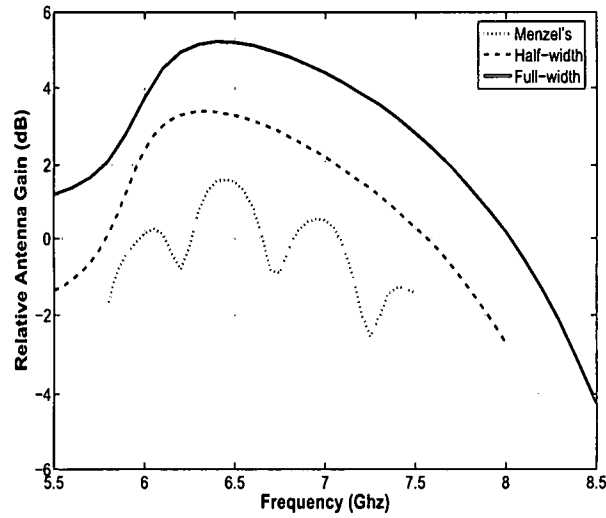


Figure 4.10: Comparison of Maximal Antenna Gain versus frequency of Menzel's, Full-width and Half-width antenna

(such as pattern, bandwidth, gain) are within an acceptable value of those at the center frequency. Fig4.10 shows the maximal antenna directivity gain of the three microstrip line leaky wave antennas (Menzel's, Full-width and Half-width) versus frequency. Clearly, the full-width configuration has the highest gain and largest bandwidth of the three leaky wave antenna configurations considered here. Furthermore, with defining the 0.5GAIN_{max} to be the acceptable gain over the whole band, the bandwidth of full-width microstrip line leaky wave antenna is around 1.7GHz. The half-width also has a wider bandwidth of 1.25GHz compared to Menzel's Antenna which has the lowest bandwidth of 0.3GHz and also the lowest antenna gain.

4.2 Computed Propagation Constant Compared with the Theoretical Analysis

In the section 3.3 of last chapter, we obtained the explicit expression for the normalized propagation constant of higher modes. Figure 4.11 shows the normalized

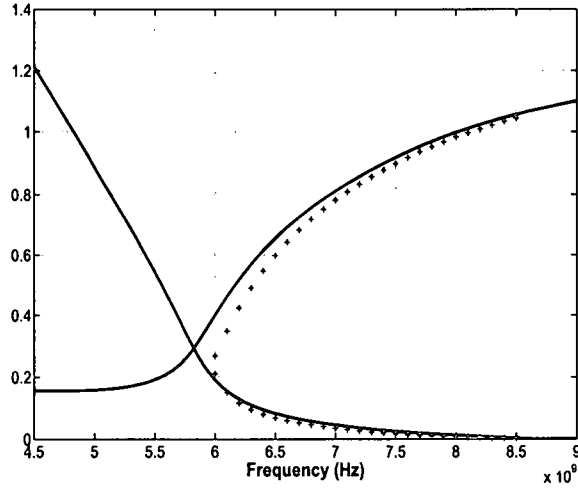


Figure 4.11: The solid blue lines represent the theoretical normalized phase constant and attenuation constant based on the Transverse Resonance Method. The red stars represent the simulation results based on the Finite Element Method (FEM).

phase constant and attenuation constant determined using the data obtained from the simulations based on the Finite Element Method and also the results obtained using the Transverse Resonance Method. The simulation is based on the full-width microstrip line leaky-wave antenna. We know the field components has an expression given by

$$E_y = e^{-k_0 z \alpha} e^{-j k_0 z \beta}. \quad (4.1)$$

The magnitude of E_y is

$$|E_y| = e^{-k_0 z \alpha}. \quad (4.2)$$

Taking the natural logarithm on both sides of eq(4.2), we obtain

$$\ln(|E_y|) = -k_0 \alpha z. \quad (4.3)$$

The slope of this line determines the attenuation constant of the first higher mode. Therefore, first from the simulation result we pull out the field component E_y along

z-axis. Then the Linear Least Squares Method can be used to estimate the slope or the attenuation constant. The formula may be expressed as

$$-k_0\alpha = \frac{n \sum (z_i |E_y|_i) - \sum z_i \sum |E_y|_i}{n \sum z_i^2 - (\sum z_i)^2}. \quad (4.4)$$

In a similar manner, the phase constant can also be estimated from the phase of the field data by the Linear Least Squares Method. From fig 4.11, we can see the theoretical analysis for complex propagation constant of the leaky modes based on the Transverse Resonance Method is very close to the estimates obtained from full-width Leaky-wave antenna simulation. Recall that the results obtained using the Transverse Resonance Method are based on Dr. Chang's papers. In conclusion, this consistency suggests that Chang's approximation and results in [11][12][13] are sound.

4.3 Field Distribution Obtained by Simulation Compared with Theoretical Analysis

In chapter 3, when we presented the theoretical analysis of the characteristic impedance for the first higher mode, we derived expressions for the transverse field components E_y and H_x of the first higher mode. The electrical field component E_y is given by

$$\begin{aligned} E_y &= \frac{1}{j\omega\mu\epsilon} \left(\frac{\partial^2}{\partial y^2} + \beta^2 \right) A_y \\ &= \frac{\beta^2}{j\omega\mu\epsilon} \cdot A_1 \sin(k_x x) e^{-jk_z z}. \end{aligned} \quad (4.5)$$

A comparison between simulation and theoretical results of E_y field distribution is shown in Figure 4.12. The operational frequency for simulation is chosen to be 6 Ghz. The fullwidth patch antenna with two symmetrical feeds structure is selected for this simulation. The location of the two feeds is at $z = -9.4375cm$ which is the beginning of the patch. The geometries and materials for the fullwidth patch antenna are given as $\epsilon_r = 2.33 - j0.0028$, patch length $l = 19cm$, patch width $w = 1.5cm$, and slab

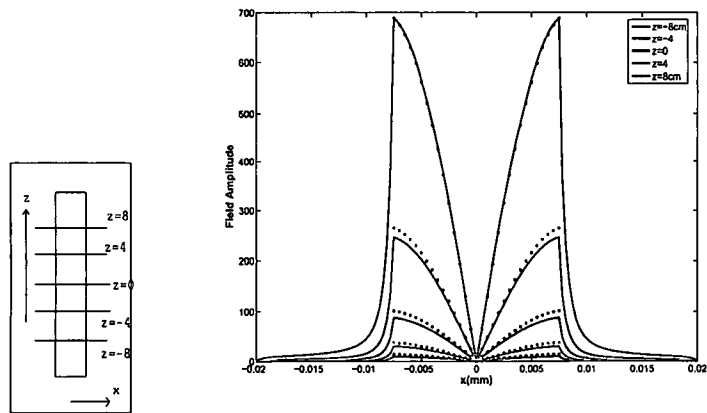


Figure 4.12: E_y field distribution:- simulation results of the fullwidth patch antenna with two symmetrical feeds structure compared with theoretical results. The stars represent the theoretical result and the solid lines represent the simulation result. $f = 6\text{GHz}$

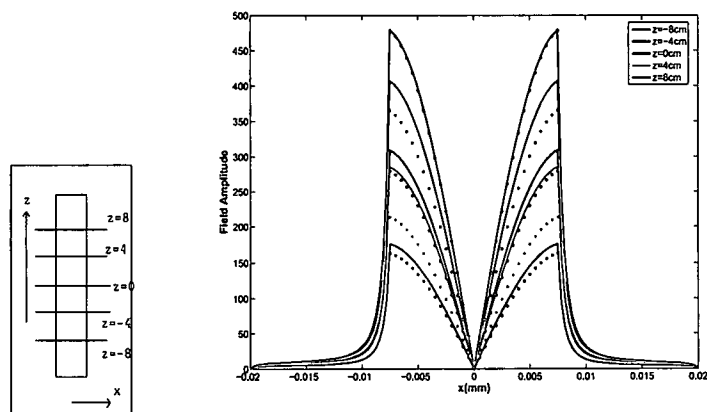


Figure 4.13: E_y field distribution:- simulation results of the fullwidth patch antenna with two symmetrical feeds structure compared with theoretical results. The stars represent the theoretical result and the solid lines represent the simulation result. $f = 7\text{GHz}$

thickness $h = 0.0787\text{cm}$. E_y , the normal component, is plotted versus x-axis which is the transverse direction. This transverse field distribution is plotted for several different positions along the direction of propagation.

From Figure 4.12, we can see that at 6Ghz both the shape and magnitude of the two results match with each other very well. With the wave propagating along z direction, the magnitude of the field decreases with increasing values of z due to the leakage of power but the shape of the field remains the same implying that only the first higher mode exists. Figure 4.13 shows another comparison corresponding to a different operational frequency of 7Ghz. However from fig[4.13] because of the existence of reflected wave only the magnitude at the first watch position of the two results match with each other well, but not at later positions. Therefore we conclude that if the attenuation constants of simulation and theory are not affected by the reflected wave or other modes, the two results should be quite close to each other and the magnitudes of the near field component should match with each other very well.

4.4 Full-Width Microstrip Line Leaky Wave Antenna with Inhomogeneous Dielectric Materials

4.4.1 Bandwidth Enhancement

In chapter 3 fig [3.5], we defined the microstirp line leaky-wave antenna's bandwidth by plotting both the phase constant and the attenuation constant in the same figure. The calculation of the phase constant and attenuation constant is based on the theory of Transverse Resonance Method. In that calculation, the width of the patch, the dielectric constant and the slab thickness were all fixed constants in order to plot the propagation constant versus the operation frequency.

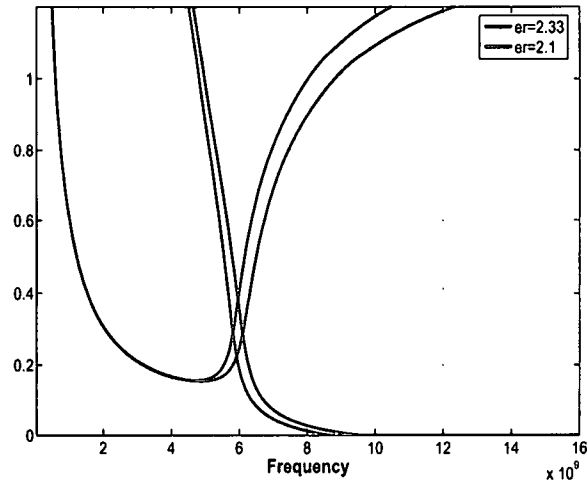


Figure 4.14: Comparing the Bandwidth of the microstrip line leaky wave antenna with different dielectric constant. $\epsilon_r = 2.33 - 0.0028$ and $\epsilon_r = 2.1$

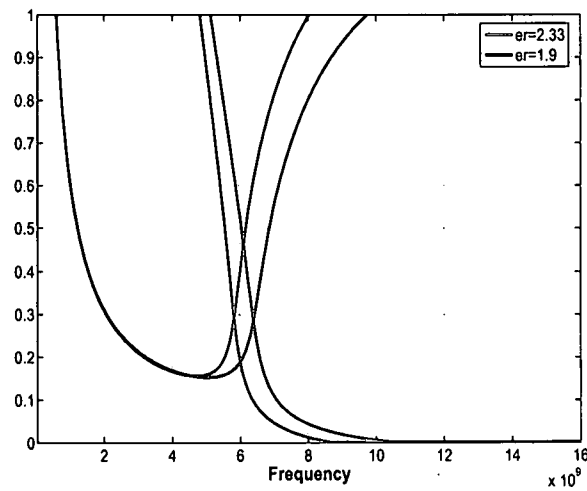


Figure 4.15: Comparing the Bandwidth of the microstrip line leaky wave antenna with different dielectric constant. $\epsilon_r = 2.33 - 0.0028$ and $\epsilon_r = 1.9$

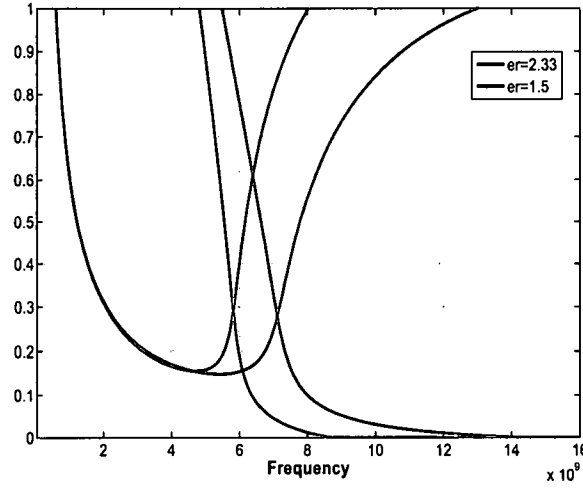


Figure 4.16: Comparing the Bandwidth of the microstrip line leaky wave antenna with different dielectric constant. $\epsilon_r = 2.33 - 0.0028$ and $\epsilon_r = 1.5$

Here we consider the effect of changing the dielectric on the bandwidth. Figure[4.14], [4.15] and [4.16] show that as the dielectric constant is decreased, for the same microstrip line, the bandwidth of the leaky wave antenna will be increased! Note that all the simulations we did previously have the dielectric constant equal to $2.33 - j0.0028$. From fig [4.16] we can infer that the bandwidth of the microstrip leaky-wave antenna with the dielectric constant $\epsilon_r = 1.5$ is much larger than the one with $\epsilon_r = 2.33 - j0.0028$.

4.4.2 Inhomogeneous Substrate Leaky Wave Antenna

In the last section, we have seen that the microstrip leaky wave antenna with the substrate of lower dielectric constant has a broader bandwidth. However, in practice we may not be able to find substrate materials that have such a low dielectric constant. Therefore, we may seek to create an equivalent substrate with a lower effective dielectric constant in order to increase the antenna bandwidth incorporating

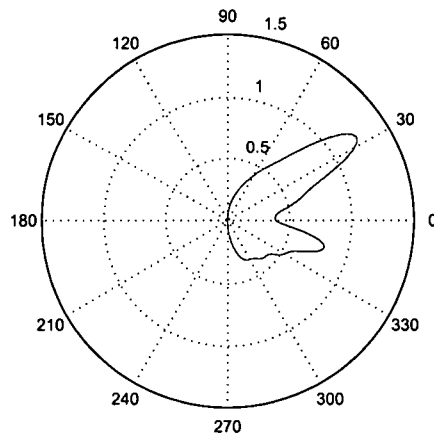


Figure 4.17: Radiation pattern of this inhomogeneous leaky-wave antenna at $f=8\text{GHz}$.
 $\epsilon_r = 2.33 - j0.0028$ and $\epsilon_r = 1.5$

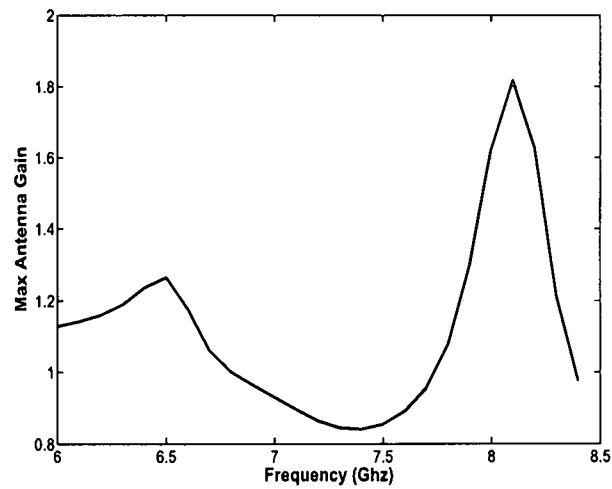


Figure 4.18: Bandwidth of this inhomogeneous leaky-wave antenna.

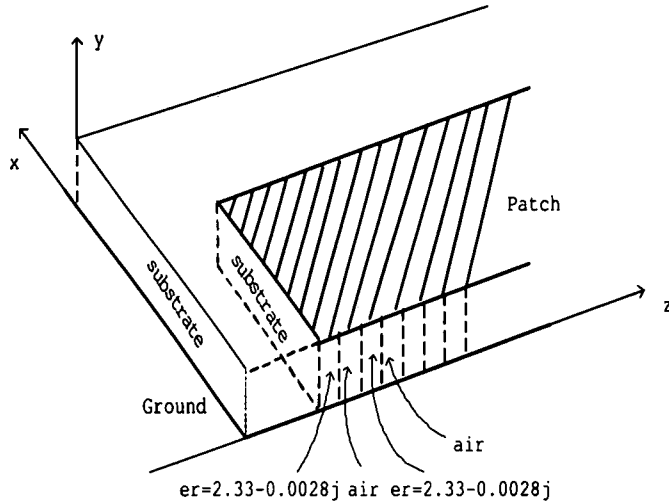


Figure 4.19: 3-D view of an inhomogeneous substrate microstrip leaky wave antenna.

appropriately designed some air holes or slots in the homogeneous substrate. Since the dielectric constant of air is 1.0 we expect that the average dielectric constant of the whole substrate will be decreased resulting in increased bandwidth. We call it inhomogeneous substrate microstrip leaky-wave antenna.

First, let us look at a simple model. We may divide the total length of patch into a few sections and we use the materials with the dielectric constant $\epsilon_r = 2.33 - j0.0028$ for the first sections. Then we put no materials (or cut an air slot $\epsilon_r = 1.0$) in the second segment. For the third segment we still has the substrate with $\epsilon_r = 2.33 - j0.0028$, and the fourth segment will be the air section (air $\epsilon_r = 1.0$) and so on (See Fig[4.19]). Here, we sought to reduce the average value of dielectric constant of the homogeneous substrate incorporating alternating regions of "high" and "low" dielectric constants. This process results in an inhomogeneous substrate. Figure[4.18] shows the bandwidth performance of this inhomogeneous substate leaky wave antenna. However, with the patch divided into 8 sections and of which four are

segments with air as dielectric the bandwidth does not improved but in fact decreases. In this case, the hoped for increase in bandwidth is not realized, because the electrical length of each section is significant; the structure behaves more like eight different and poorly matched leaky wave antennas in tandem rather than a single leaky wave antenna.

In order to make the dielectric profile smoother, we may increase the number of sections to be 20 or so such that the length of each segment is equal to 1cm. Figure[4.20] shows the bandwidth of the 20 sections inhomogeneous substrate leaky-wave antenna compared with the bandwidth of the full-width microstrip line leaky wave antenna with the homogeneous substrate. Even though the bandwidth for the inhomogeneous leaky-wave antenna did not exceed that of the full-width microstrip line leaky-wave antenna, yet it is pretty close to the bandwidth of the full-width. Secondly, the high-gain frequency band for this inhomogeneous antenna did shift to the higher frequency comparing with the high-gain frequency band of the full-width leaky wave antenna. Recall that the frequency band of the homogeneous leaky-wave antenna with a lower value of dielectric constant will move to the higher frequency according to Fig[4.16].

Therefore, following the analysis above, we may continue to increase the number of the segments to 39, which means that the length of each segment now is 0.5cm. Suppose that the operational frequency is set to be 10Ghz corresponding to a wavelength is $\lambda = 3\text{cm}$. Hence the relative length of the segment with respect to the wavelength will be $\frac{0.5}{3} = 0.167$. Figure[4.21] shows the bandwidth of this inhomogeneous substrate leaky-wave antenna and also that of full-width microstrip leaky-wave antenna which has a homogeneous substrate with $\epsilon_r = 2.33 - j0.0028$.

Defining the bandwidth to be the range of frequencies over which the relative gain is no less than 3dB below the maximum value, the bandwidth of inhomogeneous

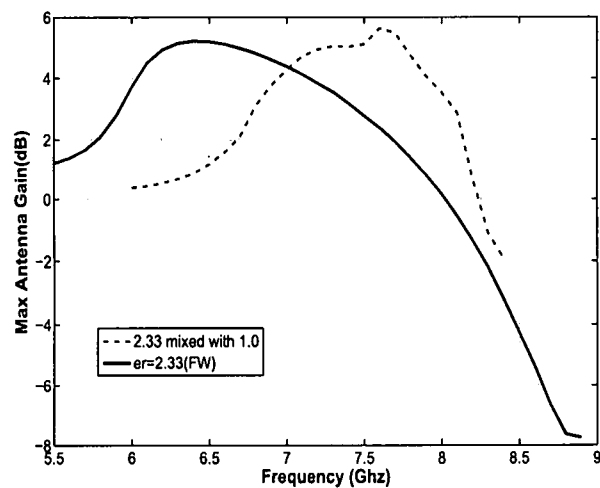


Figure 4.20:

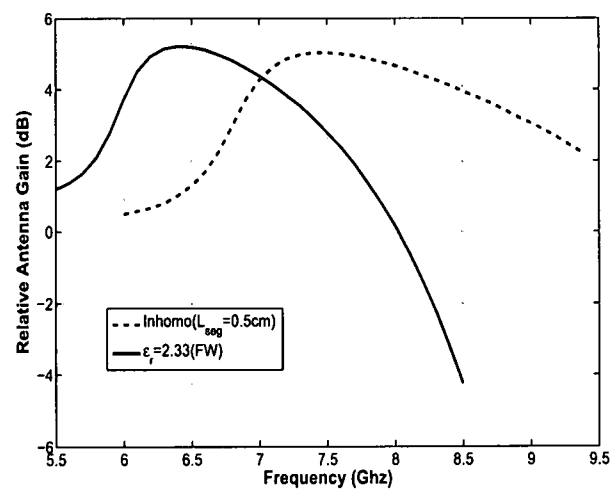


Figure 4.21: Comparison for Bandwidth of full-width microstrip leaky-wave antenna with inhomogeneous substrate leaky-wave antenna

substrate leaky-wave antenna will be around 2.5Ghz! The bandwidth of full-width microstrip line leaky-wave antenna with the homogeneous substrate $\epsilon_r = 2.33 - j0.0028$ is around 1.7Ghz which is much lower than the inhomogeneous antenna.

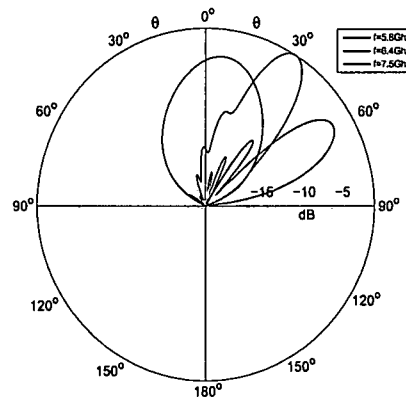


Figure 4.22: Radiation pattern of the maximal gain and two patterns of 50% gain for the homogeneous Full-width Leaky-wave antenna.

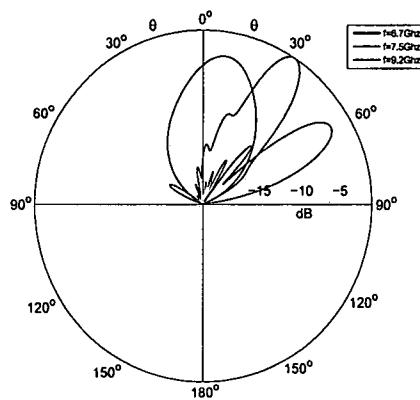
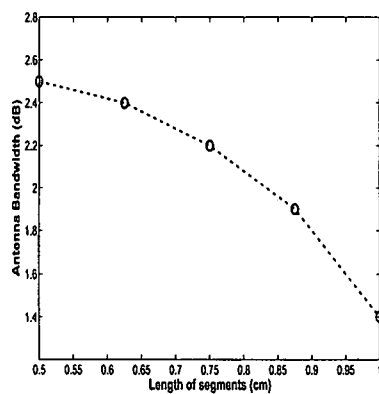
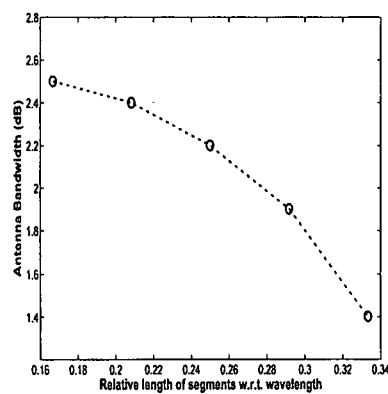


Figure 4.23: Radiation pattern of the maximal gain and two patterns of 50% gain for the inhomogeneous Full-width Leaky-wave antenna.



(a)



(b)

Figure 4.24: Inhomogeneous substrate leaky-wave antenna (a) Bandwidth versus the length of the segment. (b) Bandwidth versus the relative length of segment w.r.t. the wavelength corresponding to an operation frequency of 10 GHz.

CHAPTER 5

SUMMARY AND CONCLUSIONS

A theoretical analysis for the propagation constant, the electro-magnetic field components, and the driving impedance of the open microstrip leaky wave antenna is presented. The plot of the propagation constant versus frequencies can be used to define the bandwidth of the microstrip leaky wave antenna and also help to analyze the radiation characteristics. From the analysis of the electro-magnetic field components, we conclude that the first higher mode consists of only LSM_y mode for the open microstrip leaky wave antenna. Using the field results we could calculate the driving point impedance of the microstrip. The theoretical result for the driving point impedance is used to determine the wave and driving point impedances which used to terminate the antenna to absorb the residual power and minimize the reflections.

The Finite Elements technique based code is used as a numerical simulation tool to evaluate the fields and performance associated with the several Leaky Wave Antenna (LWA) configurations considered here. The fields and the complex propagation constant values determined using the model of a wave guide with impedance side walls agree quite well with the results obtained from the FE numerical simulations. The FE simulations have been used to evaluate the bandwidth of the three different LWA configurations as a function of the substrate dielectric constant. It is readily observed that lower dielectric constant values yield higher bandwidths, for all the three different LWA configurations.

The flexibility of the FE technique makes it possible to analyze LWA structures with an inhomogeneous profile. A number of different profiles are considered. It is shown that a periodically loaded microstrip line with alternating high and low dielectric constants (usually air), can be made, with proper choice of parameter values, to behave like a LWA with an effective homogeneous dielectric constant that is lower than the high value of the inhomogeneous LWA. This effective lowering of the dielectric results in a significant enhancement of the bandwidth.

The investigations reported here raise a number of additional questions and possibilities. Some of these are listed below:

- Since the inhomogeneous dielectric profile analyzed here may be considered to be a periodic structures, it is natural to inquire into the possibility of synthesizing a periodic transmission line with a prescribed "radiation region" and specified complex propagation constant.
- It may be recalled that the fields in the microstrip patch region can be obtained by modeling the microstrip as a wave guide with impedance walls. It is possible to control this impedance loading; indeed, it can be made to vary along the direction of propagation. The question, of course, is how can this impedance variation be harnessed to improve the performance of the LWA?
- It is also possible to electronically vary the impedance of the side wall, by incorporating novel materials such as Ferroelectric materials. It is, therefore, possible to reconfigure the LWA in real time. What should be the impedance profile?

BIBLIOGRAPHY

- [1] W. Menzel, "A new travelling-wave antenna in microstrip," *AEU*, vol. 33, no. 4, pp. 137–140, 1979.
- [2] M. L. H. M. J. H. Gregory M. Zelinski, Gary A. Thiele and A. J. Terzuoli, "Analysis of a leaky traveling wave antenna," *IEEE TRANSACTIONS ON ANTENNAS AND PROPAGATION*, 2005.
- [3] H. Ermert, "Guided modes and radiation characteristic of covered microstrip lines," *AEU*, pp. 65–70, 1976.
- [4] A. A. Oliner and K. S. Lee, "The nature of the leakage from higher modes on microstrip line," *IEEE MTT-S Digest*, pp. 57–60.
- [5] A. A. Oliner and K. S. Lee, "Microstrip leaky wave strip antennas," *IEEE*, pp. 443–446.
- [6] A. A. Oliner, "Leakage from higher modes on microstrip line with application to antennas," *Radio Science*, vol. 22, no. 6, pp. 907–912, 1987.
- [7] C.-Y. C. J.-W. S. Wanchu Hong, Tai-Lee Chen and Y.-D. Lin, "Broadband tapered microstrip leaky-wave antenna," *IEEE TRANSACTIONS ON ANTENNAS AND PROPAGATION*, vol. 51, no. 8, pp. 1922–1928, 2003.
- [8] W. Hong and Y.-D. Lin, "Single-conductor strip leaky-wave antenna," *IEEE TRANSACTIONS ON ANTENNAS AND PROPAGATION*, vol. 52, no. 7, pp. 1783–1789, 2004.
- [9] C. S. L. Pi-Wei Chen and V. Nalbandian, "Planar double-layer leaky-wave microstrip antenna," *IEEE TRANSACTIONS ON ANTENNAS AND PROPAGATION*, vol. 50, no. 6, pp. 832–835, 2002.
- [10] A. Grbic and G. V. Eleftheriades, "Leaky cpw-based slot antenna arrays for millimeter-wave applications," *IEEE TRANSACTIONS ON ANTENNAS AND PROPAGATION*, vol. 50, no. 11, pp. 1494–1504, 2002.
- [11] D. C. Chang, "Analytical theory of an unloaded rectangular microstrip patch," *IEEE Transactions on Antennas and Propagation*, no. 1, pp. 54–62, 1981.

R002592467

HECKMAN

BINDERY, INC

T 024892 E 23 00



1/19/2006

- [12] D. C. Chang and E. F. Kuester, "Total and partial reflection from the end of a parallel-plate waveguide with an extended dielectric slab," *Radio Science*, vol. 16, no. 1, pp. 1-13, 1981.
- [13] D. C. C. Edward F. Kuester, Robert T. Johnk, "The thin-substrate approximation for reflection from the end of a slab-loaded parallel-plate waveguide with application to microstrip patch antennas," *IEEE Transactions on Antennas and Propagation*, no. 5, pp. 910-917, 1982.
- [14] C. A. Balanis, ed., *Advanced Engineering Electromagnetics*. New York: John Wiley and Sons Inc., 1st ed., 1989.
- [15] C.-K. C. TZUANG, "Leaky mode perspective on printed antenna," *Proc. Natl. Sci. Counc. ROC(A)*, vol. 23, no. 4, pp. 544-549, 1999.
- [16] G. M. Zelinski, "Finite difference time domain (fdtd) analysis of a leaky traveling wave microstrip antenna," Master's thesis, Air Force Institute of Technology, 2005.
- [17] C. A. Balanis, ed., *Antenna Theory Analysis and Design*. New York: John Wiley and Sons Inc., 2nd ed., 1997.